Considerations for a Multi-Modal Electrospray Propulsion System

by

Chase Spenser Coffman

B.S., Aerospace Engineering, University of Florida (2009)

Submitted to the Department of Aeronautics and Astronautics
in partial fulfillment of the requirements for the degree of

Master of Science in Aeronautics and Astronautics

at the

MASSACHUSETTS INSTITUTE OF TECHNOLOGY

September 2012

Author .....
Department of Aeronautics and Astronautics
23 August 2012

Certified by .....
Paulo C. Lozano
Associate Professor of Aeronautics and Astronautics
Thesis Supervisor

Accepted by .....
Eytan H. Modiano
Professor of Aeronautics and Astronautics
Chair, Graduate Program Committee

Considerations for a Multi-Modal Electrospray Propulsion System

by

Chase Spenser Coffman

Submitted to the Department of Aeronautics and Astronautics
on 23 August 2012, in partial fulfillment of the
requirements for the degree of
Master of Science in Aeronautics and Astronautics

Abstract

Micro- and nano-satellites have begun to garner significant interest within the spacecraft community as economic trends encourage a shift away from larger, stand-alone satellite platforms. In particular, CubeSats have emerged as popular, economic alternatives to traditional satellites which might also facilitate low-cost space access for academia and developing nations. One of the foremost remaining obstacles to the widespread deployment of these spacecraft is the lack of suitable propulsion, which has severely limited the scope of prior CubeSat missions. While these spacecraft have gained traction by virtue of their economical size, the same quality has imposed unique propulsion demands which have continued to elude traditional thruster concepts.

The ion Electrospray Propulsion System (iEPS) is a microelectromechanical (MEMS)-based electrostatic thruster for space propulsion applications. This technology makes use of ionic liquid ion sources (ILIS) and a porous emitter substrate to obviate the need for cumbersome ancillary components and achieve the spatial and power characteristics that could lend feasibility to active micro/nano-satellite propulsion. This thesis introduces the iEPS concept and highlights the characteristics that make it attractive as a means of CubeSat propulsion. Specifically, its bimodal propulsion characteristics are presented alongside a discussion of the constant power Isp modulation mechanism that makes this unique capability possible. A simple demonstration of the variable Isp concept is reported, and a brief exploration of the performance implications is used to suggest a direction for taking it to operational maturity.

Thesis Supervisor: Paulo C. Lozano
Title: Associate Professor of Aeronautics and Astronautics

Acknowledgments

This work was supported by the National Aeronautics and Space Administration, through a NASA Space Technology Research Fellowship (Grant #NNX11AN09H), and the Air Force Office of Scientific Research.

Contents

List of Figures

List of Tables

Chapter 1

Introduction

In recent years, the satellite community has begun to explore the viability of ultra-small spacecraft as a way of relaxing the economic impact of space activities. With mission cost being ultimately linked to satellite size and mass, these spacecraft provide a natural solution to the problem of cost mitigation. Among the small satellite movement are CubeSats, a unique, and interesting, class of satellite which has gained significant developmental momentum in the last several years. Owing its incipience to a collaboration between Stanford and Cal Poly [1], the CubeSat archetype has quickly permeated the space community and currently represents the developmental focus of over 100 groups spanning governmental, industrial, and academic sectors.

The so-called 1U, or single-unit, CubeSat standard calls for a 10 x 10 x 10 cm^3 cube of approximately $1kg$ in mass, though larger architectures (namely, 2U and 3U) are also encompassed by the CubeSat umbrella. Venturini et al. [1] provide common design specifications for several of these unit sizes, some of which are reproduced in Table 1.

Table 1.1: Standard 1U and 3U CubeSat Specifications

Specifications	**Performance (1U/3U)**
Mass, kg	1 / 10
Size, cm	10x10x10 / 10x10x30
Power, W	1.6 / 10

The table provides general performance specifications for 1U CubeSats, and for the larger 3U architecture by comparison. From this basic information, it is evident that these satellites are both spatially- and energetically-limited, a fact which is rooted in their heritage as university-founded systems originally intended to serve as simple teaching platforms for students.

1.1 Basic Propulsion Relations

In order to put the limitations of ultra-small spacecraft into proper perspective, it is useful to have some basic understanding of propulsion physics. When introducing this topic, it is traditional to start by considering a generic, variable mass vehicle traveling through a force-free (i.e. free from *external* forces such as gravity) vacuum environment. This situation is, of course, idealized, but of utility in developing the most fundamental of working relations that govern the propulsion performance of actual vehicles operating in real environments.

In order to move about its environment, the aforementioned vehicle must possess some means of active propulsion, or some mechanism for generating vehicular forces that will allow it to accelerate in a desired fashion. Within the confines of free-space, the only plausible method for this propulsion is mass reaction, whereby the vehicle (or, more specifically, its engine) expels part of its own mass. By Newton's third law, the force that the vehicle imparts to expel this mass must have an equal, but opposite counterpart that acts upon the vehicle itself. This is the reaction force that the overwhelming majority of space engines leverage in creating useful propulsion for their host spacecraft.

To develop this idea in a more analytical sense, consider a control volume surrounding this theoretical vehicle, which is actively moving about its environment by continually expelling a small amount of mass at some, possibly very high, velocity. This situation is depicted in Figure 1-1, where the vehicle is traveling at a velocity $v(t)$ while its engine pushes a mass flow rate $\dot{m}(t)$ at velocity $c(t)$. Note that the velocity of the engine exhaust, $c(t)$, is measured in the vehicular frame, and not in

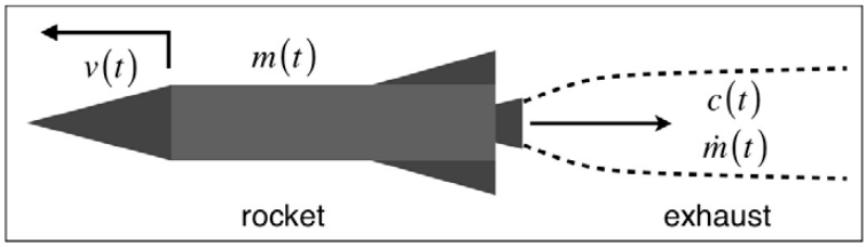

Figure 1-1: Diagram of a generic rocket [2].

that of an inertial observer.

A momentum balance can be applied to the control volume, which is *shrink-wrapped* to the body of the vehicle. It encompasses the vehicle itself, but not the exhaust, and says that

$$\sum \vec{F} = \sum \dot{m}\vec{c} \cdot \hat{n} \tag{1.1}$$

where $\hat{n}$ is the unit normal vector for the control volume surface. Since no *external* forces act on the vehicle, the left-hand of Eq. (1.1) must reduce to the thrust produced by mass reaction, which will simply be referred to as F, while the right-hand sums to the rate of momentum expulsion by the engine (unlike air-breathing engines, rocket engines have no intake). This means that the thrust force acting on the vehicle must be

$$F(t) = \dot{m}(t)c(t) \tag{1.2}$$

and, if the mass flow rate and exhaust velocity are constant, this is simply $F = \dot{m}c$. The ultimate objective in generating these forces is to take advantage of them for accelerating a vehicle in some desired way, so it is necessary to understand their correlation. Since the forces are now known, this is most readily accomplished by invoking Newton's second law of motion, $F = ma$, which states

$$F = ma \Rightarrow \dot{m}c = ma \tag{1.3}$$

where m is the mass of the vehicle, a is its acceleration, and all values are instan-

taneous. The mass flow rate being processed by the engine must be related to the total vehicular mass through $\dot{m} = -dm/dt$, which allows the equation to be recast as

$$\frac{1}{c}dv = -\frac{1}{m}dm \tag{1.4}$$

If the exhaust velocity, c, is taken to be constant, Eq. 1.4 can be integrated between initial and final masses and velocities to yield

$$\Delta\nu = c\ \ln\left(\frac{m_0}{m_f}\right) \tag{1.5}$$

or, equivalently

$$\frac{m_f}{m_0} = e^{-\Delta\nu/c} \tag{1.6}$$

where m_f is the final mass of the vehicle, m_0 its initial mass, and $\Delta\nu$ the total velocity change it experienced after thrusting with constant exhaust velocity, c. It should be noted that the difference of initial and final masses is exactly the mass of propellant, m_p, that was consumed during the impulse. The duration of this impulse is sometimes of interest, and is found to be

$$t = \frac{m_0}{\dot{m}}\left(1 - e^{-\Delta\nu/c}\right) \tag{1.7}$$

In addition, the velocity increment, $\Delta\nu$, is the actual change in vehicular velocity only if it is traveling through a force-free environment. If, by contrast, it is moving through something other than free space (e.g. in a gravitational field) there will be losses such that the change in vehicular velocity will be less, but sometimes still very near, the computed $\Delta\nu$. Regardless of the environmental situation, however, the ideal $\Delta\nu$ is that which must be used in identifying the mass ratio, from Eq. (1.6)[1]. Several important aspects of these basic motion equations can now be expounded upon:

[1] An example of a non-ideal $\Delta\nu$ maneuver is presented in Chapter 4, where it is used to highlight the advantages of variable Isp engines

1. *Mass / Velocity Changes*: Spacecraft missions are often characterized by a $\Delta\nu$ requirement. For example, raising a satellite from Low-Earth Orbit (LEO) to Geostationary Orbit (GEO) typically requires a $\Delta\nu$ of several thousand kilometers per second (roughly $4km/s$, depending upon the exact initial orbit and spacecraft). If the necessary $\Delta\nu$ is known *a priori*, the propellant mass required to execute the maneuver can be computed from Eq. (1.6) for various values of exhaust velocity, c. Conversely, if a desired propellant consumption is known, the achievable velocity increment can be found through the inverse relationship, Eq. (1.5).

2. *Specific Impulse*: Up to this point, the exhaust velocity of the vehicle's engine has simply been referred to as c. By convention, however, it is commonly referred to as the *specific impulse*, or *Isp*. For comparative purposes, the metric is sometimes expressed as a characteristic time (typically seconds) by taking its quotient with the gravitational acceleration of the Earth, g ($9.81m/s^2$). Though this interpretation possesses little physical significance, it has roots as a traditional representation.

3. *Isp Comparison*: The most important message to remember when comparing specific impulse values for various engines is that higher Isp's decrease the amount of propellant that must be expanded to realize a given $\Delta\nu$, and vice versa. Chemical engines, for example, are physically limited to Isp values beneath (approximately) 500s, while electric propulsion (or EP) engines are capable of reaching many thousands of seconds, and this has been the single greatest impetus for electric engines beginning to dominate the in-space propulsion landscape.

The final link in developing a cogent perspective for ultra-small spacecraft limitations is an understanding of power; where it comes from and how it is used by an engine to deliver useful thrust. Going back to Figure 1-1, and the idealized scenario that it depicts, conservation of linear momentum can be taken a step further to identify the so-called *jet power*, which is related to the amount of thrust produced by the

engine. Fundamentally, the *jet power* is the rate of kinetic energy deposited in the engine exhaust, and is usually expressed as

$$JetPower = \frac{1}{2}\dot{m}c^2 \tag{1.8}$$

In chemical systems, the jet power is supplied by the energy stored within the propellant itself (for example, a two-part propellant that reacts and releases thermal energy that can be transformed into kinetic energy via a nozzle), but electrical systems, in general, lack this capability. Instead, EP engines often employ inert propellants that are electrically or magnetically accelerated as power is provided through some external source. This external source is usually a battery or solar panel, which transfers energy to a power processing unit (PPU) for conditioning befure use by the engine. To account for losses along this energy pipeline, the jet power relationship, Eq. (1.8), can be recast in its more general form

$$\eta P = \frac{1}{2}\dot{m}c^2 \Rightarrow P = \frac{\dot{m}c^2}{2\eta} \tag{1.9}$$

where P is the total power input to the vehicle, and η accounts for all inefficiencies associated with the conversion from input power to useful jet power. Recalling, from Eq. (1.2), that $F = \dot{m}c$, the preceding relationship can be constructed in an even more revealing way

$$P = \frac{Fc}{2\eta} \tag{1.10}$$

which immediately indicates that low power levels limit the amount of thrust that can be generated. This, in turn, must restrict the pace at which given missions are carried out (low thrust means slow acceleration), and the situation is further worsened if the available propulsion operates with either high Isp (like EP engines) or poor efficiency.

1.2 CubeSats: *A Propulsion Quandary*

While CubeSats provide real promise for mitigating the economic impact of space access, and for possibly introducing exciting new mission paradigms (e.g. formation flight of distributed satellite architectures), the widespread deployment of these spacecraft has largely been limited by a lack of suitable propulsion options. This deficit is primarily attributable to the unique combination and spatial and power restrictions intrinsic to ultra-small spacecraft, which have proven to be a legitimate obstacle for realizing viable propulsion candidates. In particular, they seem to have precluded the possibility of employing many of the common electrical and chemical engines, at least with respect to the smallest satellites (e.g. 1U CubeSats). Scaled versions of several of these engines have previously been explored as potential suitors, but with very modest success. Aside from general performance issues concomitant to plasma thruster miniaturization, many of the traditional thruster types (both electric and chemical) require dedicated pumping and valves systems that command power of their own for actuation purposes. In the context of a spatially- and energetically-limited spacecraft, this represents an additionally burden which could potentially overwhelm the subsystem budget. Consider, for example, simple cold gas propulsion systems. Despite limited $\Delta\nu$ capability, they are simple to integrate and provide a means for active maneuvering. Like many other devices, however, they require a dedicated valve system, and this alone can consume more power (>10W, in some cases) than many 1U CubeSats are equipped to provide [3].

In light of these basic shortcomings, it is apparent that new and innovative technologies, and possibly ones which are predicated upon disparate fundamental physics, are needed to bridge the gap between the performance that current microthrusters provide, and the performance which will enable versatile CubeSat mission envelopes. The specific characteristics that these engines will need to possess can be summarized in the following ways:

1. *Small footprints*: Mass, volume, and areal footprints will need to be minimized in order to fit propulsion structures within a constrained CubeSat framework

while leaving sufficient room for payload.

2. *Low power / high energy efficiency*: Current CubeSat concepts are plagued by extreme power limitations, the effects of which were highlighted in the previous section. Economical use of available energy resources will be needed for efficacious impulsing.

3. ***Multi-Modality***: In the same spirit as that of the footprint objective, it will be advantageous for CubeSats to employ a single engine, which is capable of handling all maneuvering demands (e.g. station-keeping, collision avoidance, *and* orbit changing), in lieu of multiple, independent propulsion systems. A so-called multi-modal propulsion system is capable of operating in disparate Isp regmines, or *modes* (i.e. a high Isp mode for $\Delta\nu$-intensive maneuvers, like orbit changes, and a low Isp mode for thrust-intensive or time-critical maneuvers, like collision avoidance), and would facilitate this endeavor.

Chapter 2

Electrospray Propulsion: *Technology for a Satellite Revolution*

Among the emerging micropropulsion technologies that could meet small satellite needs is the electrospray, a unique form of electrostatic accelerator. Electrosprays distinguish themselves from other members of the electric propulsion family by virtue of their ion production mechanism. Unlike most plasma thrusters, which rely upon some form of gas-phase ionization, electrosprays extract charged particles directly from the surface of a conducting liquid propellant. This capability is facilitated by the fact that conducting fluids experience a surface instability in the presence of a sufficiently strong electric field, leading to the formation of dynamically stable, current emitting structures commonly known as Taylor cones. What makes this phenomenon so interesting, and promising, is the fact that it is intrinsic to the micro-domain. Whereas most engines must typically be scaled down for micropropulsion applications, electrosprays require some form up-scaling, and this generally precludes them from the miniaturization losses known to plague their larger counterparts.

2.1 Fundamental Physics

In 1964, G.I. Taylor described a mathematical framework for the electrospray phenomenon and showed that so-called Taylor cones are formed of a need to balance the normal electrostatic traction with surface tension forces binding the conducting fluid [4]. For a perfectly conducting fluid, and static scenario, this means that the normal field must vary like $r_C^{-1/2}$ along the body of the cone. This dependency, however, would lead to a singularity near the apex that cannot, of course, be strictly physical, and nature addresses this apparent contradiction by introducing the dynamics of charged particle emission. The specific nature of the emission is dependent upon the working fluid being used, but generally leads to the emission of charged liquid droplets, the emission of individual ions, or some combination thereof. In the case of doped organic solutions, the emission site develops the characteristic *cone-jet*, a small cylindrical protrusion from which a stream of charged droplets is issued. Liquid metal ion sources (LMIS, or FEEP), by contrast, tend to resist jet formation and emit individual ions directly from the surface of the cone, a process referred to as *field evaporation*. Ionic liquids, a relatively new class of propellant, are capable of similar evaporation when supplied at sufficiently low flow rates.

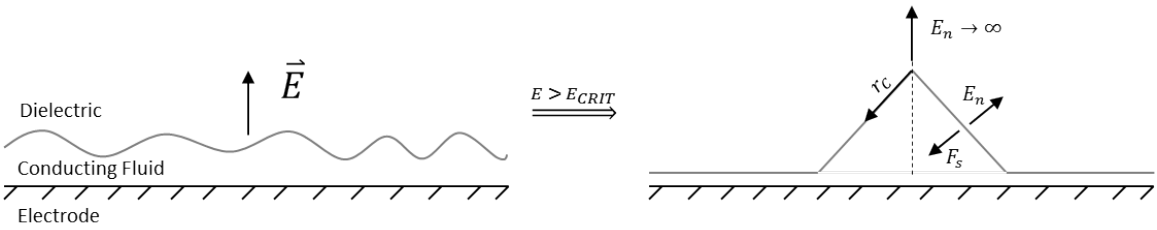

Figure 2-1: Taylor cone formation process. When the applied electric field eclipses some critical value, E_{CRIT}, the liquid surface destabilizes and snaps into a conical form where the normal field, E_n, is in static equilibrium with surface tension forces, F_s.

2.1.1 Cone-Jet Emission

Electrospray emission via the cone-jet mechanism is typically observed for doped organic working fluids (for example, LiCl in ethylene glycol), and produces streams of

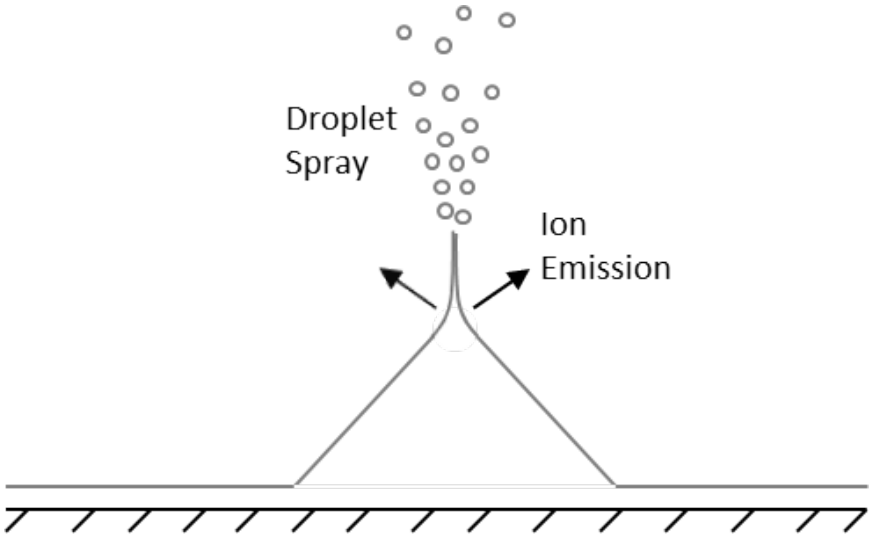

Figure 2-2: Charged particle emission via the cone-jet mechanism.

charged liquid droplets. The cone-jet itself is a thin, cylindrical protrusion extending from the apex of its Taylor cone, where the static force balance must give way, that breaks up into a fine mist of droplets that are accelerated through the externally supplied electric field. In addition to these droplets, the strong electric fields surrounding the neck of the jet can extract individual ions directly from the fluid interface, through the field evaporation process. Like the sizes of the droplets themselves, the fraction of the current carried within the resulting particle beam that is due to pure ions is related to the total mass flow of the spray, and so this parameter is usually prescribed by way of some form of external pumping mechanism.

For propulsion applications, cone-jet emission is an important phenomenon due to the fact that the droplets it generates, which are much heavier than individual ions, can produce thrust at lower Isp values. This relatively low (several hundred seconds, perhaps), native Isp can be of utility in thrust- or time-critical maneuvers, while higher Isp levels can sometimes be achieved by modulating the flow rate to increase the ion fraction, or post-accelerating the beam to higher energy levels[1]. Though intriguing, and not without significant heritage, this manner of electrospray has several drawbacks: (1) the external pumping system needed to supply the propellant

[1]Post-acceleration of droplets is similar to the Isp modulation approach (but in the opposite sense) that will be presented in a later chapter. Instead of *decelerating* relatively fast, high Isp ions, slower droplets can be *accelerated* through an additional potential.

flow places a potentially overwhelming burden on a CubeSat budget, and (2) the sometimes concurrent emission of droplets and ions leads to reduced thrust efficiency.

Polydispersive Efficiency

Anytime particles of varying charge-to-mass ratio, q/m, are accelerated side-by-side within a charged particle beam, some fraction of the supplied energy will go into heating the beam, rather than accelerating it, and therefore manifest a thrust loss. Since the velocity of each accelerating particle is related to the q/m that is possesses, particles with dissimilar ratios will travel at dissimilar speeds. This creates a relative motion among the beams constituents that leads to the well-known *polydispersive inefficiency*.

Cone-jet electrosprays are capable of concurrent emission of both ions and droplets, which makes them susceptible to polydispersive losses[2]. Mathematically, this can be understood by recalling Eq. (1.9), and invoking Eq. (1.2) to write

$$\eta = \frac{F^2}{2\dot{m}P} \tag{2.1}$$

where η is the total thrust efficiency for the engine. If the engine happens to be an electrospray that is generating a beam comprised of multiple particle families (i.e. families of particles with dissimilar q/m), the thrust contributions of each family can be summed

$$F = \sum_i \left[\dot{m}c\right]_i \tag{2.2}$$

so that Eq. (2.1) can be rewritten

$$\eta = \frac{\left(\sum_i \left[\dot{m}c\right]_i\right)^2}{2\dot{m}P} \tag{2.3}$$

This relationship can be expanded and broken into individual efficiency contribu-

[2]Simultaneous emission of both ions and droplets leads to losses, but polydispersive inefficiency is not exclusive to this electrospray mode. The emission of droplets with dissimilar q/m (which the cone-jet mechanism can also produce) or fragmentation of large ions can also lead polydispersive losses. The latter, in particular, will be discussed in subsequent chapters.

tions (power processing, energy, angular, transmission, etc. [see, for example, [5]]). For the present purposes, however, it suffices to separate the polydispersive efficiency and lump the remaining contributions together, so that variations of the former can be considered independently. Explicitly, this means

$$\eta = \eta_0 \frac{\left[1 - \left(1 - \sqrt{\zeta}\right) f_d\right]^2}{1 - (1 - \zeta) f_d} \tag{2.4}$$

where η_0 is a factor accounting for all other inefficiencies (possibly $> 85\%$ or 90%) and the second term on the right-hand side is the polydispersive efficiency, η_p. This particular formulation of η_p assumes two distinct particle families (in this case, monodisperse droplets and ions), such that ζ represents the ratio of their q/m values and f_d indicates the fraction of beam current carried by the monodisperse droplet family.

$$\zeta = \frac{(q/m)_i}{(q/m)_d} \qquad\qquad f_d = \frac{I_d}{I_d + I_i} \tag{2.5}$$

To investigate the behavior of the polydispersive efficiency, η_p, it can be plotted as functions of ζ and f_d. Since the individual efficiency contributions are multiplicative, knowing η_p will set an upper bound on the achievable efficiency and help elucidate the viability of cone-jet electrosprays for CubeSat-scale missions. Figure 2-3 delineates this behavior.

Several important trends are readily observed in the figure, namely, that η_p tends to decrease for higher values of ζ and current fractions that deviate from $f_d \to 0$ and $f_d \to 1$. Physically, this means that the more dissimilar the q/m values are for the two particle families (in this example, the larger the droplets are with respect to the ions), the worse the efficiency. Similarly, when the current is neither heavily dominated by either the droplet or ion families, the efficiency suffers in a potentially catastrophic way (e.g. 12% efficiency for $\zeta = 1000$ and $f_d = 0.02$). It is for these reasons, in addition to the fact that cone-jet emission requires a dedicated pumping system that detracts from the spacecraft budget, that this form of electrospray can

be onerous in CubeSat applications.

2.1.2 Field Evaporation

For working fluids of sufficiently high conductivity, such as liquid metals or ionic liquids, the highly-stressed meniscus of the electrified Taylor cone apex can resist jet formation entirely, and instead emit ions directly, via the *field evaporation* process. The exact physical mechanisms that underpin this phenomenon lie within the realm of molecular dynamics, a relatively young discipline, and so they have yet to be entirely understood. The kinetic theory, however, has been well-developed, and useful models are available. For example, the Schottky model for field-enhanced thermionic emission is of wide utility for its accuracy and simplicity. Mathematically, it states

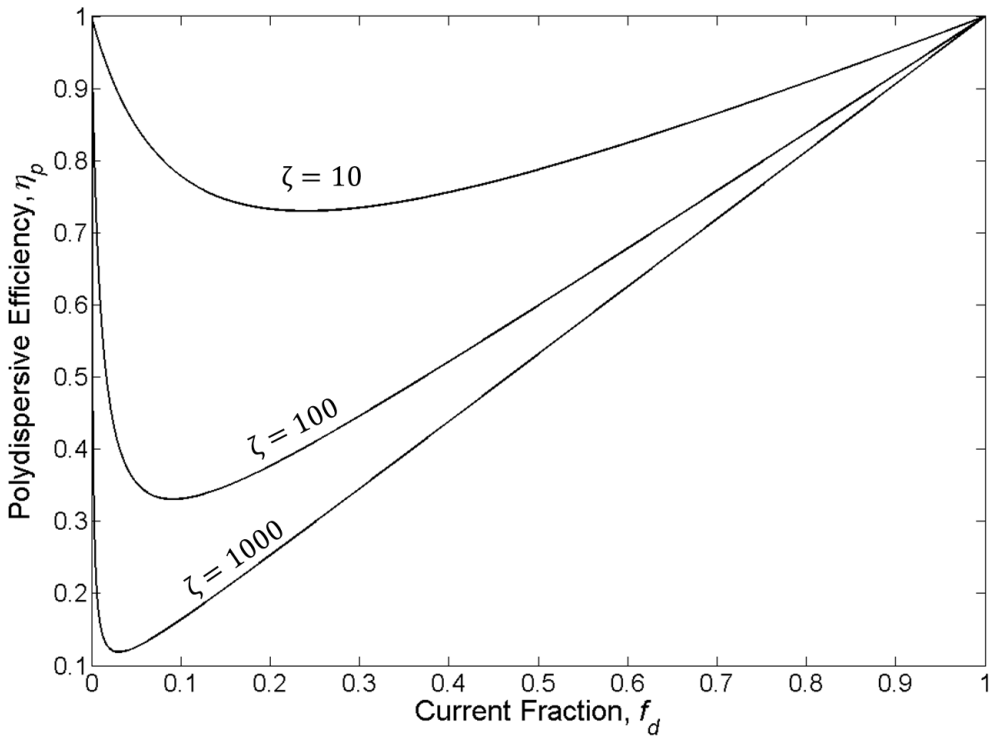

Figure 2-3: Variations in the polydispersive efficiency for a two-family ion beam. The efficiency is observed to suffer for cases where both families are present in the beam and possess disparate q/m values.

$$j = \sigma \frac{kT}{\hbar} e^{\frac{-1}{kT}\left[G_0 - \sqrt{\frac{q^3 E}{4\pi\epsilon_0}}\right]} \tag{2.6}$$

where j is the field evaporated current density, σ is the surface charge density on the electrified meniscus, k is Boltzmann's constant, T is the temperature of the fluid, $\hbar$ is Planck's constant, G_0 is the solvation energy of bound ions in the fluid (i.e. the energy barrier between ions in the gaseous and fluid states, a characteristic property of the liquid), q is the charge number of the ions, E is the magnitude of the externally applied electric field, and ϵ_0 is the permittivity of free space. Copious ion emission will occur when the externall applied field, E, begins to supply more energy to bound ions than the barrier holding them in solution, G_0. From Eq. (2.6), this is recognized to occur for vanishing (or positive) exponents, indicating that

$$E \geq \frac{4\pi\epsilon_0 G_0^2}{q^3} \tag{2.7}$$

for appreciable field evaporation. It should be noted that this manner of emission produces sprays with two distinct, and potentially advantageous characteristics:

1. *Flow rate*: The exclusive production of ions can yield relatively large currents whilst minimizing the concomitant flow rate. If some passive transport mechanism can be taken advantage of, this could potentially obviate the need for an active pump which, of course, would be spare portions of a small spacecraft's mass, volume, and power budgets.

2. *Efficiency*: Though different size ions can be emitted in this way (depending upon the composition of the working fluid), their q/m values are typically comparable because of similar sizes, and this limits inefficiency due to polydispersity.

Thrust Density Approximation

The most fundamental function of any propulsion system is to generate useful motional forces for a host craft, and so an understanding of the physical mechanisms that govern their generation, dictate their extents, and the associated limitations can

be of particular virtue. The propulsion forces generated by electrosprays are typically cast as densities (force per unit area), because of the fact that the engines created of them are highly modular and scalable (see Chapter 3). In order to explore the thrust characteristics of purely-ionic electrosprays (i.e. those which strictly rely upon *field evaporation*), a rudimentary model of a Taylor cone will be introduced so that its fluid dynamic and electrostatic properties, which govern the force generation, can be developed.

At the beginning of the chapter, it was noted that Taylor cones are formed to balance the electrostatic traction at the fluid-dielectric interface with surface tension forces in the liquid. G.I. Taylor, noted for his seminal work on these physics, found that, regardless of the properties of the working fluid, each and every cone must exhibit the exact same half-angle (49.3°) in order to satisfy the condition of surface equipotentiality. Though certain conditions can perturb this half-angle in actual emission scenarios, it has been experimentally confirmed that, in large part, Taylor cones do in fact obey this geometry. With this understanding, it is then possible to examine the strength of the normal electric field, E_n, along the boundary of the cone in order to identify the extents of the field evaporation region (recall, this phenomenon will only occur in regions where E_n satisfies Eq. [2.7]).

Consider the cone geometry depicted in Figure 2-4, where α is the so-called Taylor angle, r is the radial distance from the apex of the cone to any point (spherical coordinates), R is the radial distance of any point on the cone surface from the line

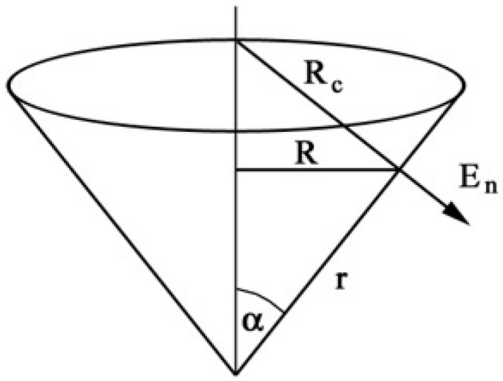

Figure 2-4: Taylor cone geometry [6].

of symmetry (cylindrical coordinates), R_c is the radius of curvature of a given point on the cone surface, and E_n is the related electric field (normal to the surface). The forces due to surface tension and electric pressure acting on a differential unit of the surface area are, in general

$$F_s = \gamma \left(\frac{1}{r_1} + \frac{1}{r_2} \right) \qquad\qquad F_e = \frac{1}{2} \epsilon_0 E_n^2 \tag{2.8}$$

The left-hand equation represents the pressure due to surface tension, where γ is the characteristic surface energy of the liquid, and r_1 and r_2 are the two principal radii of curvature, which combine to form R_c. The right-hand equation is that of the electric pressure, where ϵ_0 is the permittivity of free space and E_n is the normal electric field. Balancing the two, and noting that R_c varies like $r \tan \alpha$, it can be shown that

$$E_n = \sqrt{\frac{2\gamma \cot \alpha}{\epsilon_0 r}} \tag{2.9}$$

which describes the magnitude of the normal electric field, E_n, as a function of the radial coordinate r. Invoking Eq. (2.7), the extents of the field evaporation region can now be determined. Given the fact that typical G_0 values lie in the range from 1-3 eV [7], the evaporation condition suggests that normal electric field strengths approaching, or exceeding, $1V/nm$ are required for appreciable emission. From Eq. (2.9), this says that the field evaporation region is confined, approximately, to $r \leq 10^{-8}$ $(10nm)$, a very small area at the apex of the cone.

Unlike doped organic solvents, it was noted that higher conductivity fluids like liquid metals and ionic liquids tend to resist cone-jet formation while operating in a field evaporation mode. Instead, they likely adopt a smooth curvature at their cone apices, albeit with an extremely sharp radii. If that is the case, the properties of the small emission region can be investigated more closely using simple manifestations of the Maxwell equations.

Consider the emission region depicted in Figure 2-5, where σ is the accumulated

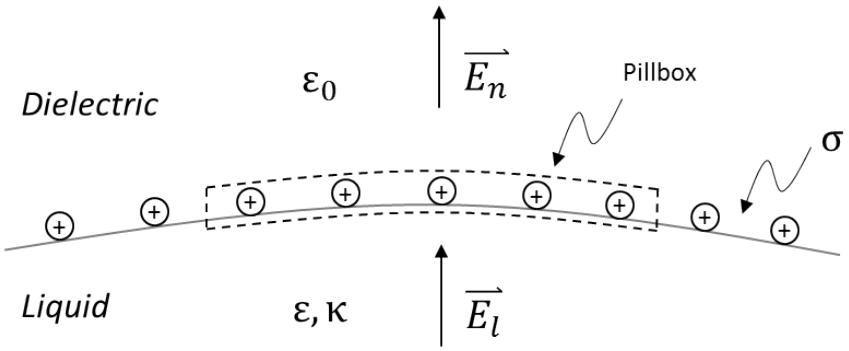

Figure 2-5: Emission surface for field evaporation.

surface charge density, ϵ and κ are the permittivity and conductivity of the fluid, respectively, E_n is the normal electric field, E_l is the electric field inside of the liquid, and the dashed control volume is a Gaussian pillbox that hugs the liquid-dielectric interface (also, a Maxwell stress tensor surface). From this simple construction, the thrust density generated in the emission region can be approximated using the Maxwell stress tensor if the internal electric field, E_l, can be found. The stress tensor says that

$$\frac{F}{A} = P_{e,net} = \frac{1}{2}\epsilon_0 E_n^2 - \frac{1}{2}\epsilon E_l^2 \tag{2.10}$$

where F/A is the thrust density and $P_{e,net}$ is the net electric pressure across the liquid-dielectric interface. Using the same stress tensor surface (in this context, it is traditionally referred to as a Gaussian pillbox), Gauss' law can be applied across the liquid boundary, yielding

$$\sigma = \epsilon_0 E_n - \epsilon E_l \tag{2.11}$$

Eq. (2.11) states that the magnitude of the surface charge density is equivalent to the difference in displacement field magnitudes across the interface. For many fluids of interest (common ionic liquids, in particular), however, an appreciable surface charge is unable to accumulate due to the fact that the time scale for flow residence is generally smaller than that for charge relaxation in the very localized emission region. This is related to typical combinations of permittivity and conductivity in

these liquids. It seems then that a reasonable approximation to the finite, but very small surface charge, would be to take $\sigma \to 0$. From Eq. (2.11), this means

$$E_l = \frac{\epsilon_0}{\epsilon} E_n \tag{2.12}$$

Substituting this into Eq. (2.10) yields

$$\frac{F}{A} = \frac{1}{2}\epsilon_0 E_n^2 \left[1 - \frac{\epsilon_0}{\epsilon}\right] \tag{2.13}$$

Typical permittivity values for ionic liquids can be on the order of $10\epsilon_0$ (or larger), which reduces Eq. (2.13), approximately, to the external electric pressure. For fields in the vicinity of $1V/nm$, this yields thrust densities on the order of $10^6 N/m^2$. To put this into perspective, the overwhelming majority of engines in the electrostatic family are limited to thrust densities near $1N/m^2$, because breakdown limitations on the allowable electric field, while magnetoplasmadynamic engines (MPDs), which are amongst the most powerful EP devices, operate at high magnetic pressures on the order of $10^4 N/m^2$. The caveat to this argument, of course, is related to the fact that the ion emission region occupies but a small fraction of the total cone area, and so electrosprays will never *quite* be able to reach such high thrust densities. However, the fact still remains that if very dense cone arrays can be generated within an electrospray engine, to achieve even a fraction of this maximum theoretical thrust level, it would represent a *quantum leap* in electric propulsion performance. Unlike MPDs, which tend to be extremely bulky and inefficient, these electrospray devices would be small, lightweight, highly efficient, and likely inexpensive. This is the *revolution* that has electrospray physicists and engineers so excited.

2.2 Electrospray Architectures

Up to this point, the electric field needed to engender electrospray emission has simply been "externally applied", but real devices require some feasible architecture for providing it and, in addition to the particular working fluid or emission type, this

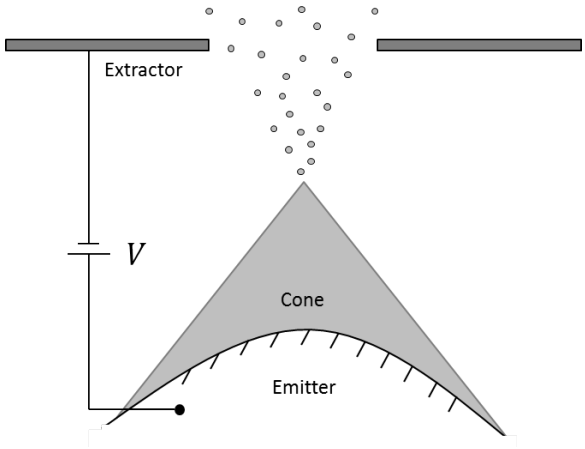

Figure 2-6: Electrospray schematic depicting the necessary structural and electrical components for propulsion. These include a wetted emitter structure, a power supply, and a perforated extractor.

has become another distinguishing feature amongst genres of the technology. In the context of propulsion, the electric field necessary to destabilize the fluid surface and accelerate ions is generally supplied by neighboring electrodes that are biased in a way similar to that of parallel plate capacitors. One of these electrodes is wetted with the propellant, and, to facilitate emission at modest potentials, usually comprises some manner of sharp geometric feature known as an *emitter*. The emitter serves to amplify the local electric field and anchor the emission site(s) so that the ion beam that it produces can be guided through a perforation in the opposing, or extractor, electrode. This provides the momentum flux that generates thrust, as depicted in Figure 2-6.

Individual emitters can usually provide no more than a small fraction of a μN (usually 10s of nN)[3], and so large numbers of them are typically arrayed to generate useful propulsion forces[4]. Within these arrays, emitters have typically manifested themselves as capillaries, for fluids of non-negligible vapor pressure, or needle-like structures that are externally-wetted, for liquid metals and ionic liquids. Several examples are depicted in Figure 2-7.

[3]Note that this is more-or-less consistent with the thrust approximation developed in the previous section, particularly if an individual emitter is capable of supporting the formation of *multiple* Taylor cones.

[4]This is in the spirit of the cone-densification that was motivated in the previous section.

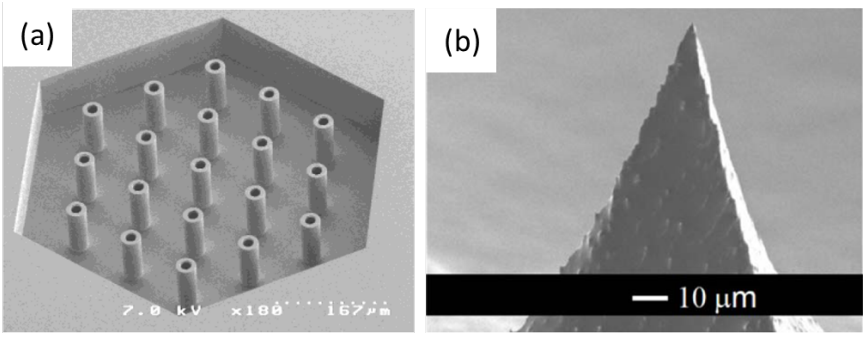

Figure 2-7: Images of a capillary emitter [8], left, and an externally-wetted emitter [9], right.

2.2.1 Porous Electrospray Emitters

While both capillary and externally-wetted emitters lend themselves to modern micromachining techniques, when fabricated from silicon, at least, they each possess specific deficiencies and drawbacks. Capillaries, for example, often suffer from cross-talk issues, clogging, and overflow failure while externally-wetted emitters exhibit saturation currents that are limited by poor propellant transport. In contrast, porous-type emitters have been investigated more recently as a way of allaying some of these problems. By virtue of their porous structure, they naturally avoid clogging and saturation issues by providing a network of flow paths, and alleviate cross-talk through enhanced fluidic impedance between neighboring emitters. An example of a porous emitter structure is shown in Figure 2-8.

In addition to the aforementioned characteristics, porous emitters provide another, and very important, capability that could be an enabling feature for active

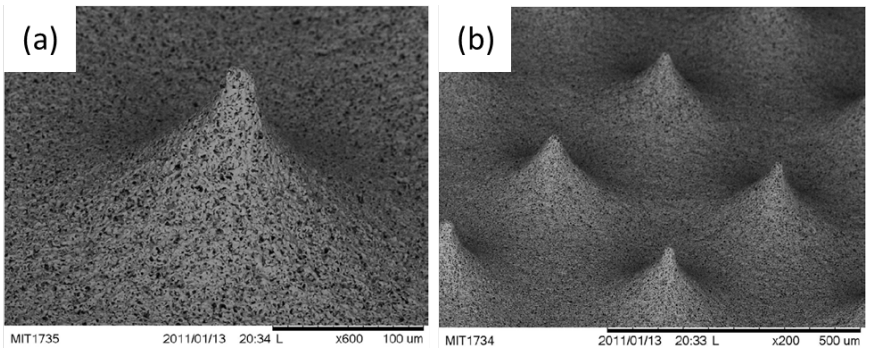

Figure 2-8: Examples of porous emitter structures [10].

small satellite propulsion: if the flow rate is small enough, they can deliver propellant via capillarity alone. While certain emission regimes (e.g. the droplet regime) require active pumping to achieve typical spray properties, others are less restrictive. In particular, the purely ionic emission regime of ionic liquid propellants is characterized by low enough flow rates for capillarity to become a viable propellant delivery mechanism, and this wholly eliminates the need for cumbersome pumping and valve systems. As a result, porous electrosprays are promising profound mass, spatial, and power benefits that have made them exciting candidates for CubeSat propulsion applications.

Chapter 3

The ion Electrospray Propulsion System: *An Overview*

The ion Electrospray Propulsion System (iEPS) is a microelectromechanical systems (MEMS)-based electrospray thruster for space propulsion applications being developed in the Space Propulsion Laboratory (SPL) at the Massachusetts Institute of Technology. It features a porous metal emitter substrate and operates within the purely ionic emission regime of ionic liquid propellants (i.e. it relies on field evaporation) in order to obviate the need for cumbersome ancillary components like electrical pumps and valves, but also possesses the highly meritable capability for viariable Isp performance. The variable Isp capability is facilitated through the use of multiple electrostatic optics, and allows the system to operate in both high Isp (low thrust) and low Isp (high thrust) propulsion modes. In addition to the footprint benefits afforded by capillarity-driven propellant feeding, this provides significant budgetary savings through the elimination of any need to incorporate redundant maneuvering mechanisms. A schematic of the concept is presented in Figure 3-1 (a).

The figure depicts several key components of the iEPS concept, as well as their relative positioning. The basic structure is composed of a 2D array of porous emitters, atop of which sits an assembly of two electrostatic grids. The intermediate grid, or extractor, interacts with the emitter tips to generate ion beams while the (optional) downstream grid, the accelerator, modulates the associated energy. The device is

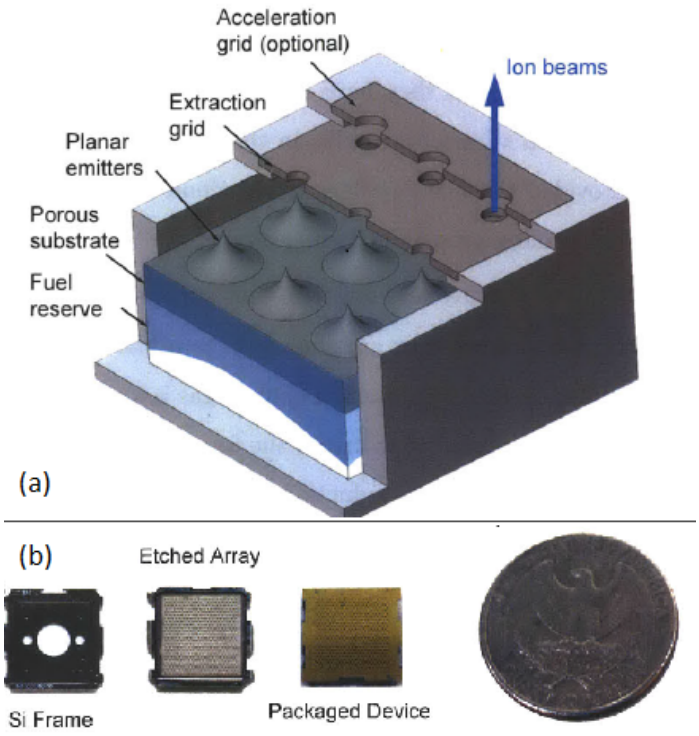

Figure 3-1: Schematic of iEPS concept, top, and images of the proof-of-concept platform, bottom.

capable of operating with a single grid, but two are needed in order to function as a variable Isp system.

3.1 iEPS v1: *Conceptual Validation*

The initial iteration of the iEPS concept was a proof-of-concept platform that was used to demonstrate techniques for manufacturing large arrays of porous metal emitter tips (480 individual tips, in this case), and for confirming the potential for the high current throughputs that distinguish porous emitters from their externally wetted counterparts. Images of the individual components for this iteration are shown in the bottom of Figure 3-1, with a quarter depicted for reference. Using the proof-of-concept device, Courtney [11, 10] conducted detailed studies of various fabrication techniques and mapped baseline performance metrics for 2D porous electrosprays, several of which are referenced in Table 3.1.

While the Courtney studies were restricted to single-grid iEPS thrusters, the re-

sults were exciting in that they demonstrated the feasibility of manufacturing high fidelity, fully 2D porous emitter arrays and confirmed the potential for attractive propulsion performance[1].

Table 3.1: Baseline iEPS Performance

Thruster Metric	**Design Goal**	**Actual**
Dimension (mm)	–	12x12x2.3
Weight (g)	<1	0.7
Peak Current (μA, per emitter)	1.0	>1.0
Peak Power (W)	<1.0	0.7
Isp (s)	>2000	2000-3000

3.2 Thruster Scaling

Though the proof-of-concept made use of 480 individual tips spaced across an area of less than 1 cm^2 (corresponding to an emitter pitch of 450 μm and a packing density of 2 emitters/mm^2), denser arrays are not precluded by the capabilities of the technology or its physics. In fact, from a performance perspective, denser arrays can be very advantageous, and not in small part due to the reasons outline in Chapter 2. For devices like the iEPS, de-sparsification can be realized in one of several ways, two of which will be presented here.

3.2.1 Photographic Scaling

Photographic scaling of electrospray devices can be desirable because it affords improved thrust performance, while mitigating the device footprint simultaneously, but also lends convenience in that the layout of the device is completely conserved (relative positioning, architecture, etc. are all the same); the device is simple scaled by a single, consistent factor. Legge [12, 13] attempted to quantify the benefits of this densification approach by posing the theoretical performance of porous electrospray

[1]For detailed studies and a review of iEPS v1 emission characteristics and performance, see [11, 10]

thrusters in terms of the emitter pitch and specific mass, volume and area characteristics (by thrust), which are relevant metrics for power-limited small satellites. The results are reproduced in Table 3.2 where d, the emitter pitch, represents the scaling variable.

Table 3.2: Photographic Scaling of Porous Electrosprays

Thrusters	**d, μm**	**$\tilde{m}$, g/mN**	**$\tilde{V}$, cm^3/mN**	**$\tilde{A}$, cm^2/mN**
Tungsten ILIS array	300	8.33	8.03	10.13
	100	0.31	0.30	1.13
Nickel ILIS array	300	6.32	–	–
	100	0.23	–	–
Typical ion engine	–	91	109	7.7
Low-power Hall thruster	–	156.3	63	6.25

The findings indicate that porous electrospray arrays of only slightly larger density than the iEPS proof-of-concept compare very favorably to similar EP engines that have been explored for small satellite applications in the past. More exciting, perhaps, is the fact that there is no intrinsic restriction to packing below the smallest pitch depicted in the table, $100\mu m$, which could help lead to lead minute thrusters possessing thrust (density) performance rivaling even the most powerful EP engines. This, of course, is the ultimate goal of any nascent technology, and future iEPS generations will attempt approach this possibility by pushing the limits of densification by way of photographic scaling.

3.2.2 Direct Emitter Densification

In contrast to photographic scaling, direct densification involves the simple infusion of additional emitter structures to an existing electrospray framework without affecting the packaging. For example, the iEPS v1 could be directly densified by increasing the number of active tips from 480 to 1000+, while conserving the exact same silicon package (i.e. more tips could be etched into the porous metal surface without changing the chip or frame dimensions). If the emission properties are conserved for increasingly

small pitch scales[2], then the emitter density and thrust performance should both scale like $pitch^2$.

Unlike photographic scaling, direct emitter densification possesses very obvious limitations. The first, and likely the most restrictive, is mechanical in nature and involves the well-known phenomenon of *electrostatic pull-in*. When two electrodes are placed in close proximity and provided a relative bias, the field that is generated in the inter-electrode space must give rise to an attractive force that works to pull them together[3]. If the voltage is held constant, and one of the electrodes lacks enough support to keep it from deforming a small amount, an instability can occur in which the two are completely collapsed upon one another. For a simple parallel-plate capacitor, the voltage at which this will occur is described by

$$V_p = \sqrt{\frac{8}{27}\frac{kd^3}{\epsilon A}} \tag{3.1}$$

where k is the mechanical stiffness of the moving plate (this assumes that the other is perfectly rigid), d is the initial electrode separation, ϵ is the dielectric permittivity, and A is the electrode area. For electrospray devices, the emitter array and perforated extractor grid are analogous to the plates from the capacitor; the array is fixed while the grid, which is generally very thin[4], is free to deform or deflect under the influence of the applied electric field. During direct densification, the addition of new emitters necessitates the inclusion of new perforations in the extractor grid which, of course, must weaken it[5]. In general, the more holes it has, the more compliant it will be, and this affects the k value that characterizes the system in such a way as to decrease the pull-in threshold, effectively limiting the feasible emitter density.

A second, and possibly less restrictive limitation is related to propellant transport

[2]This seems to be the case, at least within a reasonable range of pitches that extends, possibly, down to 10's of microns. See [12, 13] for a more detailed discussion.

[3]This comes from traction on the surface charge, like that which was described in thrust density calculations from the previous chapter

[4]Extractor grids are typically designed in such a way as to be as thin as possible, in order to mitigate ion beam interception. The consequences of this interception are expounded upon in the next chapter.

[5]Fortunately, this problem has already been studied to some extent in the literature, and models for effective plate modulus in terms of the perforation size and density are available [14, 15]

within the emitter bodies. For decreasing emitter pitch, the bodies of the emitters themselves must also decrease in scale and this can have implications for their fluidic impedances. While this issue is not likely encumbering for pitches within the realm of mechanical feasibility (i.e. those that are permitted by the structural considerations), it is academic to take note of.

Though firm limitations are concomitant to direct densification, devices like the iEPS v1 are well within their thresholds. As a consequence, significant performance improvement can be made before the need for global dimensional scaling is required, and this convenient avenue should be pursued in the near-term. After exploring the mechanical behavior of perforated plates in more detail, it is possible that the physics will be found to permit in excess of 2000 emitters, which would constitute a four-fold increase in density. Given that current thrust performance is close to 0.25 N/m^2, this increase would already put the present device in the company of full-scale ion engines, which is no small feat.

3.3 Fabrication Techniques

Electrospray devices require one or more well-defined, and often very sharp, emitter structures in order to properly perform, and the ultimate goal of the fabrication process is their realization in a consistent, repeatable, and accurate way. Depending, however, on the selected emitter material, whether or not a single emitter or an array is to be created, the desired architecture, and the intended application, the quality of the end-product can be decidedly influenced by the particular method used to create it. The identification of a feasible approach, therefore, is less than trivial. For an idea as to how these obstacles have been tackled in the past, several techniques which have accrued appreciable heritage in the electrospray propulsion community are enumerated below:

1. *Electrochemistry*: Electrochemical techniques have previously been used in the fabrication of both single and arrayed emitters, particularly when the foundational material is a metal. This approach involves the immersion of the

emitter precursor (the base material) in an appropriate chemical bath, with the inclusion of a counter-electrode that is capable of being selectively biased. Depending upon the emitter material and choice of chemical electrolyte, an externally applied voltage can be used to control the rate at which the emitter material is machined, and intricate 3-dimensional structures can result, particularly when this process is employed with photolithographically-defined masking agents. Examples of this include [12, 13], in addition to the iEPS v1 work detailed by Courtney [16, 10].

2. *Dry Etching*: For certain material selections, wet etching (such as electrochemistry) provides ill-defined results. Silicon, for example, is a popular emitter material that is not conducive to wet techniques. It does, however, lend itself to dry etching processes, which is particularly convenient because of the fact that the IC (Integrated Circuit) industry has already invested a great deal of time and money in developing high-fidelity methods. These include Reactive Ion Etching (RIE), the Deep Reactive Ion Etching variation (DRIE)[6], and Ion Milling, among others. Examples of dry-processed electrosprays include [8, 17, 9].

3.3.1 iEPS Manufacturing

Early in the iEPS design process, metal emitter materials were identified for their utility in supporting electrospray emission, in addition to their availability in porous formats. This section briefly introduces the transformation of these materials (porous nickel, in the iEPS v1 case) into high-fidelity emitter arrays that are contained within flight-like packaging. The topics discussed herein are intended to be an overview, and the reader is referred to the literature [16, 10] for a much more intricate examination of the processes.

An overview of the basic manufacturing steps is shown in Figure 3-2, indicating that the process starts by seating a blank, porous metal chip in a pre-fabricated

[6]This method is designed for extreme directionality (approaching complete anisotropy), which contrasts with its more basic RIE relative.

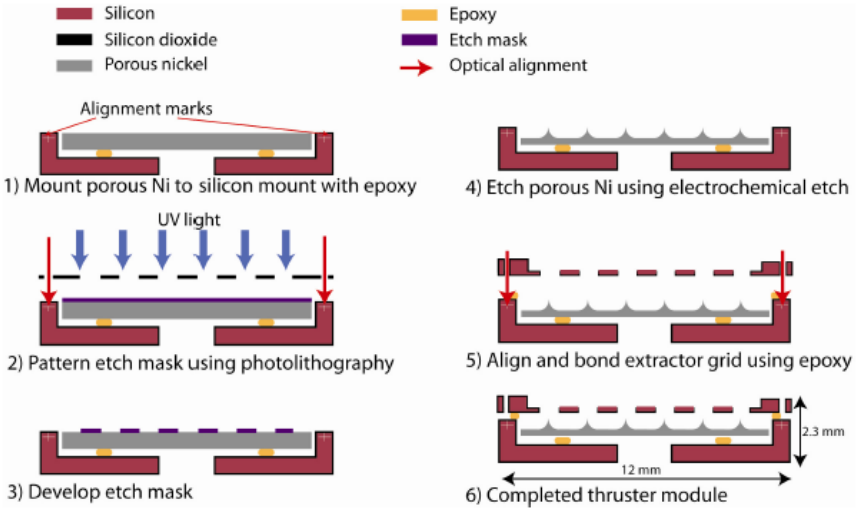

Figure 3-2: Process sequence for iEPS fabrication [18].

silicon frame. For the first iteration of iEPS devices, this chip was a piece of 10 x 10 x 1 mm^3 porous nickel. The assembly is then transported to a clean room facility and laminated with a strip of dry photoresist before patterning with standard photolithographic techniques. This process results in a triangular dot array that serves to define the sizes and locations of the emitters that will be machined in a later step. It should be noted that while current devices make use of a dot pattern with 450 μm pitch, future work will reduce this in the interest of the added performance described earlier in the chapter.

Emitter tips are etched into the patterned assembly by subjecting it to electrochemistry. For nickel substrates, a hydrochloric acid electrolyte (2.0 N) is used, and the micromachining process is carried out in a special etching station designed by Courtney, and described in detail in the references [10]. The merit of this station is a moveable counter electrode (paddle) that provides control of the electrolyte hydraulics. Specifically, it facilitates etching within a transport-limited regime that has been shown to yield a high degree of emitter-level uniformity [16, 10]. Figure 3-3 shows several images of the emitter tip structures that are produced with these techniques, and highlights the level of achievable uniformity.

The left side of the figure depicts a uniform array of 480 emitter tips, while the right is a zoomed view of an individual tip. Figure 3-3(b) highlights the rounded

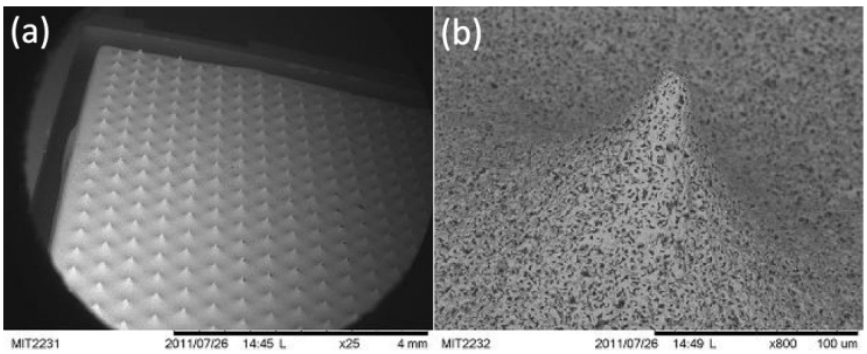

Figure 3-3: Examples of iEPS emitters. Left, an array of electrochemically etched porous emitters, and right, a zoomed view of a single structure. These results highlight the level of sharpness and uniformity that electrochemistry provides.

apex, approximately 15 μm in radius, that make these tips conducive to effective electrospraying. The small curvature also facilitates Taylor cone formation at modest potentials (< 1000V), and helps steer the resulting spray through the corresponding perforation in its extractor.

Chapter 4

Multi-Modal Electrosprays: *Propelling CubeSats to the Moon, and Beyond*

In order to execute the most interesting missions, both high thrust and high Isp propulsion systems are typically required to maneuver a satellite in the necessary ways. While the high Isp engine is relied upon to impart the bulk of the necessary $\Delta\nu$, given the more modest propellant requirements, the high thrust engine provides greater agility for time-critical maneuvering.

Given the inherent difficulties in integrating propulsion with the smallest of satellites (e.g. CubeSats), designers are becoming increasingly aware of the challenge that they would face in attempting to employ distinct systems for the panoply of different maneuvers a versatile spacecraft might perform. It seems that the most convenient, and plausible, solution to this issue could be one in which a single propulsion system handles all $\Delta\nu$ responsibilities within a given mission. For this system to be effective then, it would need to have the capability for operating in both high Isp and high thrust modes. Engines that can operate in this way are typically referred to as multi-modal propulsion systems and, in the context of power-limited applications, generally achieve their flexibility through some form of variable Isp mechanism.

An Example of Variable Isp Utility: *Spiral Climbing*

While multi-modal propulsion systems possess the very attractive benefit of consolidating distinct $\Delta\nu$ functions, their variable Isp capabilities could potentially give rise to additional advantages such as real-time, on-orbit Isp optimization and maneuver expediting. To highlight these aspects, a simple CubeSat maneuver will be explored in order to contrast the performance levels of fixed and variable Isp engines.

The maneuver to be executed is a spiral climb, one of the most basic low-thrust EP missions, between a shallow 250 km altitude LEO orbit and one at 500 km. Within this atmospheric region, drag forces for CubeSats are still on the order of 10's of μN (not entirely small compared to the thrust levels delivered by power-limited EP engines) and so increased $\Delta\nu$ requirements are generally expected for these spacecraft as they combat drag. To see why, consider the non-dimensionalized equations of orbital motion shown below

$$\frac{d^2\hat{r}}{d\hat{t}^2} - \hat{r}\left(\frac{d\theta}{d\hat{t}}\right)^2 + \frac{1}{\hat{r}^2} = \hat{a}_r \tag{4.1}$$

$$\hat{r}\frac{d^2\theta}{d\hat{t}^2} + 2\left(\frac{d\hat{r}}{d\hat{t}}\right)\left(\frac{d\theta}{d\hat{t}}\right) = \hat{a}_\theta \tag{4.2}$$

where the non-dimensional variables are

$$\hat{r} = \frac{r}{r_0}$$

$$\hat{t} = t\sqrt{\frac{\mu}{r_0^3}}$$

$$\hat{a}_r = \frac{a_r}{\mu/r_0^2}$$

$$\hat{a}_\theta = \frac{a_\theta}{\mu/r_0^2}$$

For spiral climbs, the radial acceleration, $\hat{a}_r$, is approximately zero while its azimuthal counterpart, $\hat{a}_\theta$ is

$$\hat{a}_\theta = \frac{D/m}{\mu/r_0^2}\left[\left(\frac{F}{D}\right) - 1\right] \tag{4.3}$$

in situations where there is a drag force, D, acting on a satellite which provides its own thrust, F. Since the ratio of drag forces to gravitational forces (the multiplicative factor on the right-hand side of Eq. [4.3]) is known, these non-dimensional equations can be integrated between circular orbits at 250 and 500 km, with F/D as a parameter, in order to identify conditions in which drag forces might significantly impact maneuvering. Before doing so, however, it will be useful to manipulate the F/D parameter in order to express it in a more appropriate way for the small spacecraft being considered, which are typically characterized in terms of their power levels rather than the thrust that they deliver. Invoking Eq. (1.10), F/D can be written

$$\frac{F}{D} = \psi = \frac{2\eta P}{cD} \tag{4.4}$$

Figure 4-1 shows the results of these integrations, with the necessary $\Delta\nu$ depicted as a function of the non-dimensional thrust, ψ. Although it was assumed that the drag remained relatively constant throughout the climb, which is not strictly the case, the findings are nevertheless enlightening in that they reflect the notion that spacecraft with limited power should have a harder time maneuvering in LEO, because of drag effects. From the curve, it is evident that the required $\Delta\nu$ climbs asymptotically, for $\psi \to 1$, toward an infinite velocity increment[1]. For small spacecraft with fixed Isp engines performing in the vicinity of 3000s, this ψ range (ψ <5) represents power levels below roughly 4W, suggesting that CubeSats could be hindered.

While power-limited, fixed Isp engines might be susceptible to drag forces in LEO, their variable Isp counterparts possess an innate defense; they are capable of *decreasing* their Isp at lower altitudes, to gain additional thrust and overcome drag, and then slowly increasing it again as they climb in order to leverage the propellant economy of high Isp. To highlight this advantage, the maneuver simulations can be performed

[1]Recall, from Chapter 1, that the *ideal* $\Delta\nu$ is not necessarily equal to the actual change in spacecraft velocity, but is the relevant value for computing the propellant requirement.

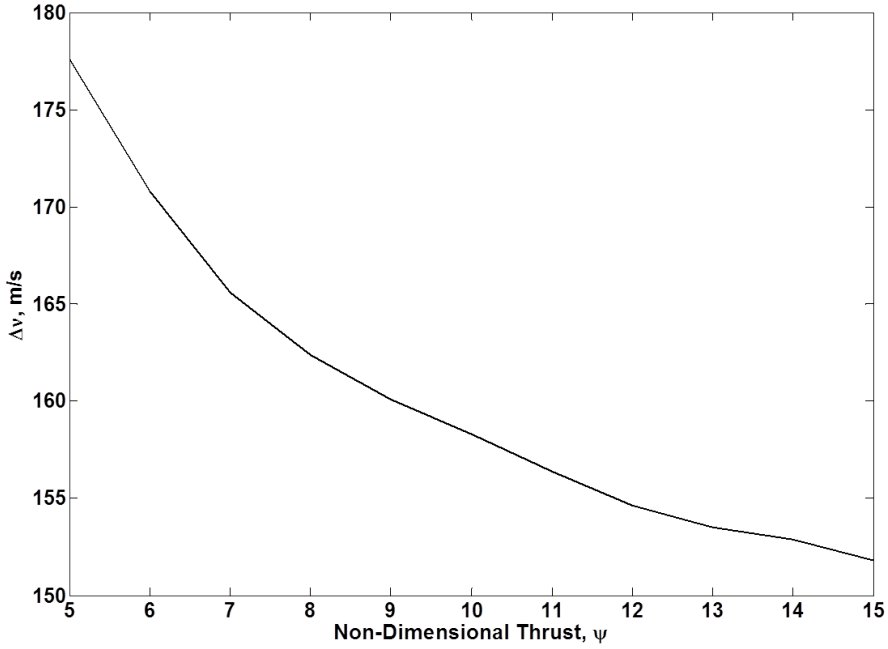

Figure 4-1: Changes in $\Delta\nu$ with drag. Notice that low values of ψ lead to high $\Delta\nu$ requirements while large values of ψ asymptote toward the theoretical minimum for EP.

once again, but this time using both fixed and variable Isp engines. For the purpose of this simple demonstration, these hypothetical engines will operate with $P = 1W$, $\eta = 0.9$, $Isp = 3000s$ (corresponding to $\psi = 1.13$, for the fixed engine), and a linear Isp profile for the variable device[2].

The results of these simulations are presented in Table 4.1. When the available power is fixed *a priori*, as it is with a CubeSat, only a single mission time exists for a fixed Isp engine, and this is reflected in the data along with a steep $\Delta\nu$ penalty that is due to drag. Note that the drag-less result would have been

$$\Delta\nu = \sqrt{\frac{\mu}{r_0}} - \sqrt{\frac{\mu}{r_1}} = 142m/s \tag{4.5}$$

In contrast to the fixed case, a range of mission times are afforded by a variable

[2]The Isp will vary, approximately, between $v_{ch} - \Delta\nu$ and v_{ch} over the duration of the maneuver, where v_{ch} is the well-known Stuhlinger velocity. For drag-free maneuvers, this type of Isp variation is known is to be ideal [19, 20], though in case its use implies a degree of sub-optimality. Nevertheless, it will serve as a helpful tool for reinforcing the present argument.

Isp engine, and it is observed that some of these are *both* less time consuming and more fuel efficient, a direct result of the ability to circumvent drag losses through Isp tailoring. The conclusion here is that variable Isp engines possess a decided advantage over their fixed performance counterparts. While consolidating distinct $\Delta\nu$ requirements and limiting the number of necessary propulsion elements a spacecraft must carry, they also afford the ability to directly an Isp profile to a given mission. The flexibility that this provides is unparalleled, and the performance improvements that this facilitates are what might ultimately power CubeSats to places like the moon, and beyond.

Table 4.1: Climbing Performance for Fixed and Variable Isp Engines on a 1U CubeSat

	Fixed Isp	**Var Isp** #1	**Var Isp** #2	**Var Isp** #3
$\Delta\nu$ Requirement, m/s	229	184	159	147
Propellant Mass, g	7.6	7.3	10.7	27
Maneuver Time, $days$	43.9	30	15	5

4.1 Variable Isp Electrospraying

Future generations of iEPS devices will incorporate variable Isp functionality in order to operate in both high thrust and high Isp propulsion modes. This capability will eliminate the need for complimentary propulsion systems and reduce the propulsion footprints, adding feasibility to dynamic small satellite missions.

In the context of electrospray thrusters, variable Isp performance is achieved by way of a second electrostatic optic, or accelerator, as depicted in Figure 3-1. The function of the dual-grid architecture is to effectively decouple the energy of the emitted ion beam from the current that it carries. What this also means is that the beam energy, which dictates the Isp, can be modulated independent of the power being consumed by the thruster. In other words, constant power Isp modulation is permissible, and this of added benefit in power-limited applications where it is desirable to take full advantage of available energy resources throughout the duration

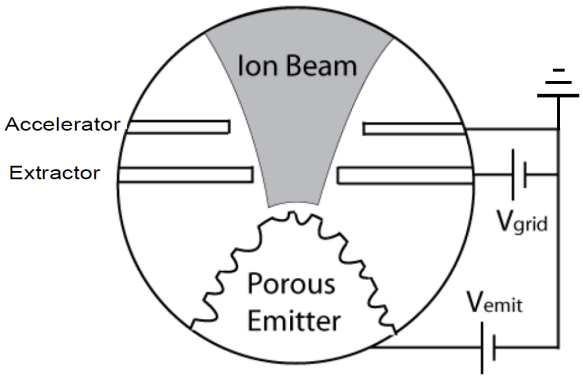

Figure 4-2: Schematic of a dual grid electrospray architecture. The downstream grid, or accelerator, serves to decouple the energy of the beam from the current that it carries, which facilitates constant-power Isp modulation.

of a mission. A more detailed schematic of a dual-grid electrospray system is shown in Figure 4-2.

To better understand the physical underpinnings of the constant power, variable Isp mechanism, the physics that dictate the performance of electrospray devices can be briefly examined. As outlined in Chapter 2, cone formation and incipient electrospraying occurs when the applied electric pressure destabilizes the exposed surface of the conducting liquid propellant. For a porous emitter, this occurs when the electric pressure reaches the capillary pressure. Mathematically, this means

$$\frac{1}{2}\epsilon_0 E_{CRIT}^2 = \frac{2\gamma}{r} \tag{4.6}$$

where E_{CRIT} is the critical field and r is the characteristic radius of a pore. Beyond incipient emission, it is well known that the current throughput continues to grow in proportion to the applied field. By contrast, the energy of the beam that carries this current is proportional not to the applied field, but to the net potential through which it falls. This is related to the fact that charged particles must obey an energy balance between their electric potential and kinetic energies. In general, this balance says

$$q\phi_0 + \frac{1}{2}m_0 v_0^2 = q\phi_1 + \frac{1}{2}m_1 v_1^2 \tag{4.7}$$

where ϕ, m, and v are the local potential, mass, and velocity, respectively. Using this relationship, the velocity of the exhausted particles can be recast as

$$c = \sqrt{2\frac{q}{m}V_{NET}} \tag{4.8}$$

where c is the Isp (m/s) and V_{NET} is the net potential through which the charged particles fall. Since the Isp of EP engines is tantamount to their exhaust velocity, the conclusion here is that it must only be a function of the net potential applied between the emission site and the exhaust, whereas the current is sensitive to the applied field. If the net potential can be decoupled from the field affecting the emitter, this means that the current and Isp can be controlled separately. Going back to Figure 4-2 now, this is seen to be the purpose of the second grid. To clarify this point, Figure 4-3 depicts a representative distribution of potentials for a variable Isp system.

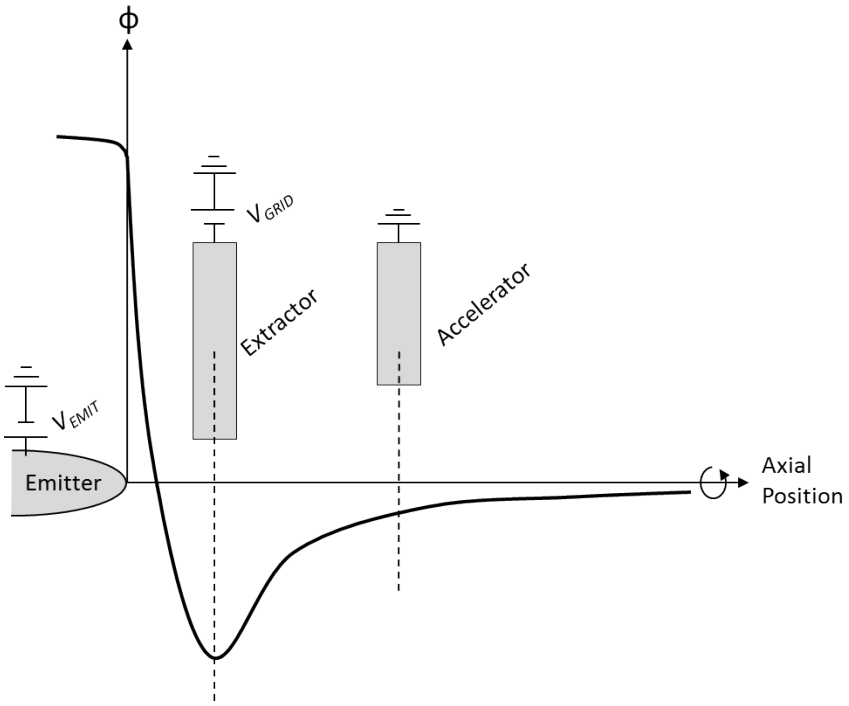

Figure 4-3: Representative potential distribution within a dual-grid electrospray. V_{EMIT} sets V_{NET} directly while the applied field is controlled through $V_{EXT} = V_{EMIT} - V_{GRID}$.

4.2 Performance Implications

The primary function of a variable Isp propulsion system is to provide both high thrust and high Isp maneuvering capabilities for a satellite, by operating in disparate Isp regimes, and eliminate the need for redundant systems that would otherwise occupy some part of the mass and spatial budget. In power-limited situations, where it is advantageous for the propulsion system to operate at constant power, the necessary Isp variation is achieved by way of the direct exchange of thrust for the exhaust velocity of emitted particles. To see why this must be the case, consider the power consumed by the thruster [Eq. (1.10)]

$$P = \frac{Fc}{2\eta} \tag{4.9}$$

where P is the total power consumption, F is the thrust, c is the particle-averaged exhaust velocity, and η is the efficiency. For the power to remain constant, it is clear that the thrust must vary inversely with the Isp when it is modulated.

In the high thrust mode, propellant consumption is sacrificed in the interest of reduced maneuver times by dropping the operational Isp. From Eq. (1.10), it is seen that this reduction in Isp engenders a proportional increase in F. Given that maneuvering times are generally prescribed *a priori*, there must be a need then to understand the way in which they are impacted by the level of thrust supplied by the propulsion system. For ideal cases that are free from external forces, this relationship can be elucidated by considering the equation of motion that governs the vehicular acceleration

$$F = ma = \dot{m}c \tag{4.10}$$

where a is the acceleration and m is the instantaneous mass given by

$$m(t) = m_0 - \int \dot{m} dt \tag{4.11}$$

Assuming that the $\Delta\nu$ impulse is performed at constant thrust and constant Isp,

Eq. (4.10) can be integrated, while noting that $\dot{m} = -dm/dt$, and combined with Eq. (4.11) to find

$$t_m = \frac{m_0 c}{F}\left(1 - e^{-\Delta\nu/c}\right) \tag{4.12}$$

where t_m is the maneuver time and m_0 is the spacecraft mass prior to thrusting. The equation says that, for a fixed Isp, the time to complete a $\Delta\nu$-constrained maneuver is inversely proportional to the amount of thrust provided by the propulsion system. What has been noted, however, is that in a constant power (as opposed to constant Isp) situation, the thrust that can be supplied is related to the Isp at which it is delivered. It might be of more use then to describe the mission time as a function of the Isp alone. This can be done by invoking Eq. (1.10), so that

$$t_m = \frac{m_0 c^2}{2\eta P}\left(1 - e^{-\Delta\nu/c}\right) \tag{4.13}$$

The point of interest now is determining the variation of this mission time for different levels of thrust/Isp supplied by a constant power system. Assuming a variable Isp thruster can execute a given maneuver by delivering thrust at two different levels of Isp, at a nominal level of c_0 and at a reduced level of c, the ratio of their associated maneuvering times is

$$\frac{t_m}{t_{m,0}} = \left(\frac{c}{c_0}\right)^2 \left[\frac{1 - e^{-\Delta\nu/c}}{1 - e^{-\Delta\nu/c_0}}\right] \tag{4.14}$$

For $\Delta\nu << c$, this ratio is linear in c/c_0, but otherwise varies in a complex way. The relationship is plotted in Figure 4-4, with $\Delta\nu/c_0$ as a parameter. For clarity, the related ratio of propellant consumption is also shown.

From the figure it is evident that wide modulation of the Isp (i.e. reduction of the Isp to very small values) can significantly reduce the amount of time needed to perform a maneuver. Specifically, it is seen that the maneuvering time approaches zero for the same limit in c. From Eq. (1.10), $c \to 0$ is tantamount to $F \to \infty$, but this cannot, of course, be physically permissible. In the case of electrosprays, the discrepancy is reconciled by the efficiency of the device, which was neglected in the

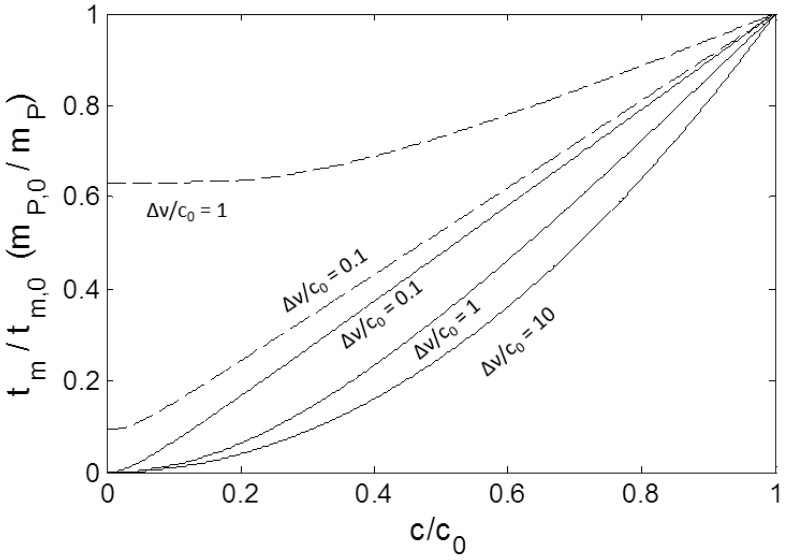

Figure 4-4: Ideal variations in mission time, t_m, with Isp, c. The dashed curves represent the related variations in propellant consumption.

formulation of Eq. (4.14). More generally then, it can be modified to reflect these additional variations, so that

$$\frac{t_m}{t_{m,0}} = \left(\frac{\eta_0}{\eta}\right)\left(\frac{c}{c_0}\right)^2\left[\frac{1-e^{-\Delta\nu/c}}{1-e^{-\Delta\nu/c_0}}\right] \tag{4.15}$$

which says that losses in efficiency at low Isp can counteract gains in the maneuvering time. For the $\Delta\nu/c_0 = 0.1$ case, the ratio of maneuvering times is plotted in Figure 4-5, with the efficiency ratio as a parameter now.

From the figure, strong efficiency losses are seen to have a decidedly negative impact on the effectiveness of Isp modulation. In particular, it is noted that these losses can actually *increase* the amount of time required to execute a maneuver, in some cases. The mechanism for this result, from Eq. (1.10), has to do with the fact that an efficiency loss can reduce the amount of deliverable thrust, even when the Isp is dropped, and this is a direct contradiction of the intended modulation purpose. In order for multi-modal propulsion systems to provide the highest level of mission flexibility, it is clear that they must be capable of operating with minimal efficiency variations over a broad range of Isp. To ensure this, some understanding of the loss mechanisms for variable Isp electrsprays is required.

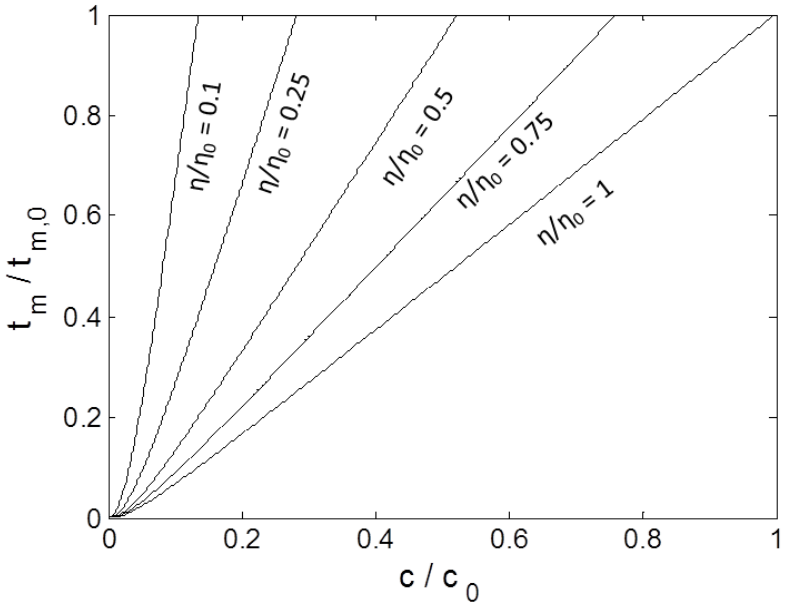

Figure 4-5: Variations in mission time with modulated Isp and non-ideal efficiency. When the Isp is dropped, reductions in engine efficiency are seen to negatively impact maneuvering performance. Note that the regions of each curve above $t_m/t_{m,0} = 1$ (not shown here) indicate operating points in which the mission time increases.

4.2.1 Dual-Grid Efficiency

For electrosprays, the most important form of efficiency loss at lower Isp values is related to the interception of some part of the emitted ion beam by the electrostatic grids. At relatively modest Isp levels, and above, very good beam transmission (near unity) is generally achievable [21]. Below some threshold, however, the fraction of the beam that is transmitted must always decrease and, to see why, the nature of the ion optics, with particular respect to those of ionic liquid beams, can be considered. It is well known that electrosprayed ion beams are characterized by some distribution of particle energies, which is a result of the fact that certain molecules within the beam are prone to fragmentation [22]. For optical configurations like the dual-grid electrospray that is being developed, ion beams with disperse energy profiles present problems for two reasons: (1) the potential distribution through the grid system can have a focusing effect, but only for particles of a specific energy; all other energies are scattered to varying degrees, and (2) in order to escape the system, a given

particle must possess an energy that is tantamount to, or greater than that of the net potential drop, V_{EMIT}. If the beam is characterized by a broad energy distribution it is likely that the strong acceleration/deceleration needed for low Isp operation will inflict significant beam scattering, leading to direct grid impaction. Similarly, these broad distributions mean there will be particles in the beam that do not possess enough energy to climb the potential barrier between the extractor and accelerator. This will become more clear in the next section, where beam modulation experiments are presented.

To see how beam interception will influence the efficiency of a dual-grid device, a simple power balance can be examined. For an electrostatic electrospray accelerator this can, in general, be written

$$\eta = \frac{P_{JET}}{P_{IN}} \tag{4.16}$$

where η is the total device efficiency, P_{IN} is the externally supplied power, and P_{JET} is the familiar jet power. Combining Eq. (1.8) with Eq. (1.2), this is recast in the more useful form

$$\eta = \frac{F^2}{2\dot{m}P} \tag{4.17}$$

In general, the thrust contributions of individual particle families are summed so that

$$F = \sum_i \dot{m}_{i,p}\, c_{i,x} \tag{4.18}$$

where $\dot{m}_{i,p}$ and $c_{i,x}$ are the mass flow and axial velocity of the exhaust, respectively, which are related to the total values through the efficiencies η_{TR} and η_θ. Explicitly

$$\dot{m}_{i,p} = \eta_{TR}\dot{m} \qquad\qquad c_{i,x} = \eta_\theta c_i \tag{4.19}$$

The present purposes are only concerned with variations in the device efficiency as

the Isp is modulated, which should not be significantly impacted (from a qualitative standpoint, at least) by the presence of multiple particle families. In the interest of simplicity then, a single family can be assumed for Eq. (4.18), while noting that the existence of additional families can be easily handled by introducing the familiar polydispersive efficiency term, η_p. Referring back to Eq. (4.17), these say

$$\eta = \eta_{TR}^2 \eta_\theta^2 \eta_p \frac{\dot{m}c^2}{2P} \tag{4.20}$$

From Eq. (4.8), the relationship between the Isp (i.e. the exhaust velocity, c) and the applied emitter potential can be invoked, though an appropriate energy efficiency, η_E will be introduced here[3]. Additionally, the mass flow rate is related to the prevailing current through the charge-to-mass ratio, $\dot{m} = I(q/m)^{-1}$, which, when substituted for, yields

$$\eta = \eta_{TR}^2 \eta_\theta^2 \eta_p \eta_E \frac{IV_{EM}}{P} \tag{4.21}$$

where V_{EM} is the emitter potential. As mentioned earlier, the purpose for this exercise is elucidating qualitative efficiency trends with respect to grid impaction and the modulation of Isp, which should not be directly influenced by the η_θ, η_p, or η_E[4] terms. They can, therefore, be lumped into a *baseline* efficiency term, η_0, that is recognized to be within the vicinity of 85%+ for many ionic liquids. In contrast, the power term in the denominator can be expanded to reveal its contributions, which come from *both* the emitter and extractor power supplies. The power being consumed by the emitter supply is obvious, but it is also important to recognize that, should any current intercept the (biased) extractor, it too will need to consume power in a way that will impact the total device efficiency. Explicitly, the total power consumption is

[3]The energy efficiency describes the impact of the ion cost, which is typically on the order single volts for many ionic liquids. This term is, in general then, very high ($\geq 95\%$).

[4]Because the ion cost is fixed, η_E should rapidly increase for small Isp values, but this will not be considered here.

$$P = IV_{EM} + I(1 - \eta_{TR,EX})V_{EX} \tag{4.22}$$

where V_{EX} is the bias on the extractor grid and $\eta_{TR,EX}$ is its local transmission fraction, which is related to the *total* transmission fraction, η_{TR}, through

$$\eta_{TR,EX} = 1 - \frac{I_{EX}}{I} \quad \text{and} \quad \eta_{TR,AC} = 1 - \frac{I_{AC}}{I} \Rightarrow \eta_{TR} = \eta_{TR,EX} + \eta_{TR,AC} - 1 \tag{4.23}$$

and $\eta_{TR,AC}$ is the related fraction for the accelerator. Note that $\eta_{TR} \leq \eta_{TR,EX}$ in all cases. Going back to Eq. (4.21) now, the expanded power term can be substituted to yield

$$\eta = \eta_0 \frac{\eta_{TR}^2}{1 + (1 - \eta_{TR,EX})\,\nu} \tag{4.24}$$

where ν is the ratio V_{EX}/V_{EM}. At this point, Eq. (4.24) roughly describes the device efficiency in terms of the pertinent transmission fractions and a factor ν, the physical meaning of which has yet to become clear. From a basic understanding of the system at hand, it makes sense that ν should somehow relate to the power and Isp, so it would be beneficial to describe it in those terms. To do this, it is first observed that in a practical setting the value of the emitter potential, V_{EM}, would be set in order to prescribe a desired Isp, while the extractor potential (which was noted to directly control the current) would be tailored in order to satiate a given power requirement. This suggests that V_{EM} should only relate to the Isp then, and Eq. (4.8) can be invoked to yield

$$\nu = \frac{2\eta_E}{c^2}\left(\frac{q}{m}\right)V_{EX} \tag{4.25}$$

so that all that is left is to relate V_{EX} to the power consumption. Recalling Eq. (4.22), it is seen that an expression for the current, I, is needed to complete the relationship. For electrosprays of the present type, it is well known that the current throughput scales linearly with the applied field after incipient emission at

some start-up voltage, V_{ST} [11, 10]. A useful phenomenological relationship for this behavior is

$$I = \alpha \left(V_{EM} - V_{EX} - V_{ST} \right) \tag{4.26}$$

where α is an empirical factor relating the current throughput to the applied voltage (amperes *per* volt), and $V_{EM} - V_{EX}$ is the relevant emission that is modified by the start-up potential. Substituting this relationship into Eq. (4.22), and attempting to find a close-form solution for V_{EX} in terms of the power seems to be intractable, however. While the process would provide a convenient non-dimensional number that could be used to explore efficiency variations over c, P, η_{TR}, and $\eta_{TR,EX}$ in an expedient way, a more feasible, but equally as enlightening approach is adopted here. It is to

1. Select a nominal operating point: c and P which are in the vicinity of native conditions for a single-grid electrospray.
2. Select an extractor transmission of interest, $\eta_{TR,EX}$.
3. Select a total tranmission of interest, η_{TR}.
4. From Eq. (4.8), identify the necessary emitter potential, V_{EM}.
5. From Eqs. (4.22) and (4.26), identify the necessary extractor potential, V_{EX}.
6. Formulate the potential ratio, ν.
7. From Eq. (4.24), compute the device efficiency.
8. Return to (1), (2), and (3) to investigate variations in c, P, η_{TR}, and $\eta_{TR,EX}$.

Following the outlined process permits the formulation of families of efficiency maps that are useful in determining qualitative trends among the engine parameters (specifically, c and P). An example of particular interest to the present discussion is the possibility for constant-power curves that delineate changes in efficiency over a

modulated Isp, with the trasmission fractions as parameters. To generate these here, the following values can be taken

$$c_0 = 2500\text{s}$$
$$P_0 = 1\text{W}$$
$$V_{ST} = 1000\text{V}$$
$$\alpha = 1\mu\text{A/V}$$

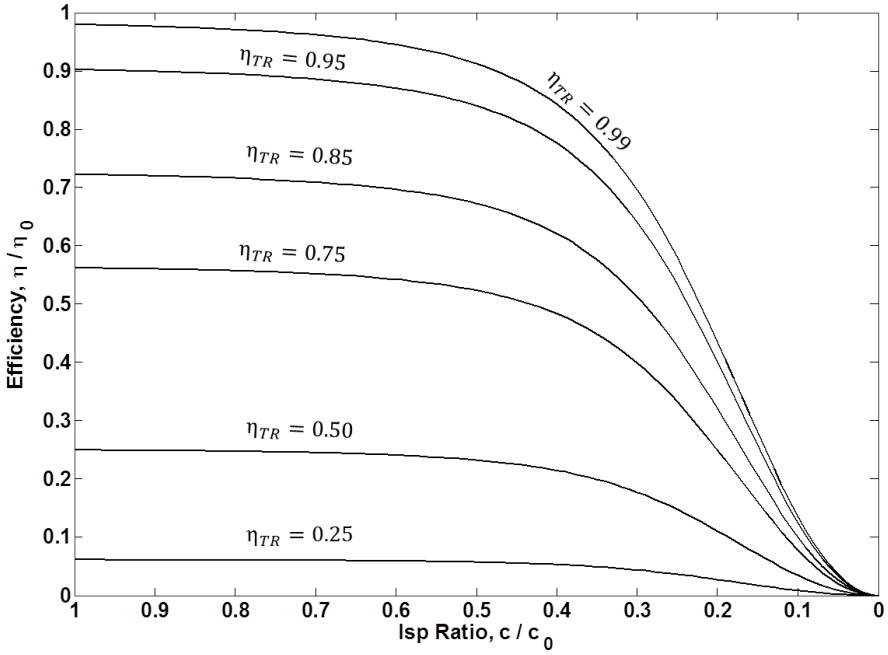

Figure 4-6: Dual-grid efficiency variations with Isp and η_{TR}. The transmission $\eta_{TR,EX}$ is fixed.

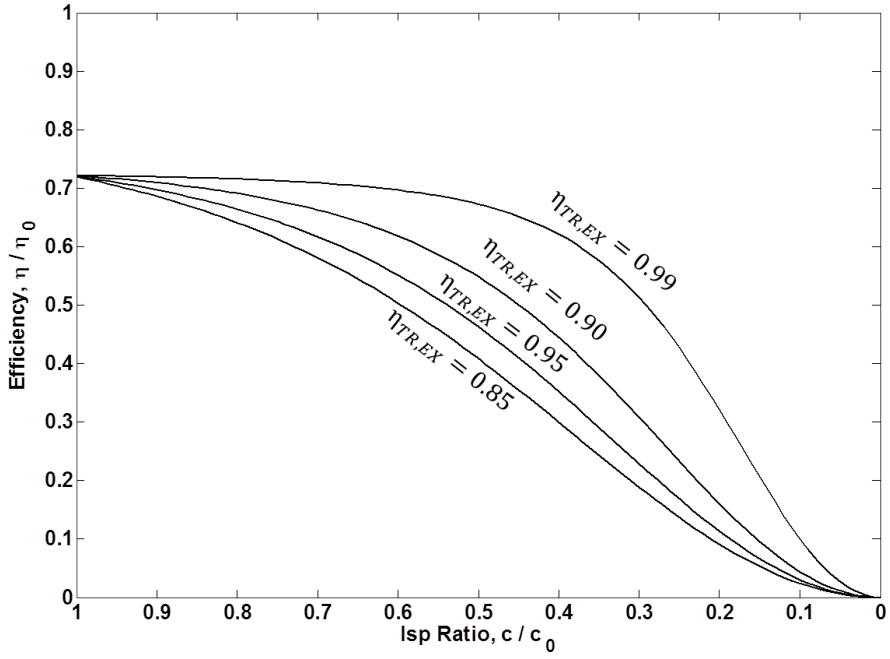

Figure 4-7: Dual-grid efficiency variations with Isp and $\eta_{TR,EX}$. The transmission η_{TR} is fixed.

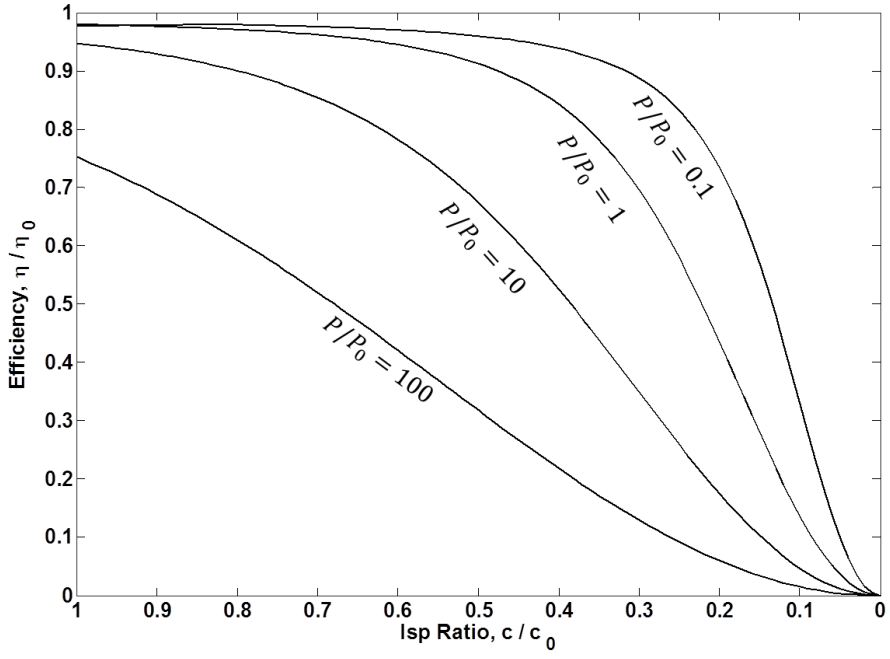

Figure 4-8: Dual-grid efficiency variations with Isp and power. The transmissions η_{TR} and $\eta_{TR,EX}$ are fixed.

All figures depict efficiency variations over changes in the Isp. Each, however, is representative of different paramters, according to the schedule

Figure 4-6: $\eta_{TR,EX} = 0.99$

Figure 4-7: $\eta_{TR} = 0.85$

Figure 4-8: $\eta_{TR} = \eta_{TR,EX} = 0.99$

Note that in all cases, save for Figure 4-8, the curves represent constant-power variations. Several qualitative observations can now be made about the behavior that they reveal:

1. *Variations in* η_{TR}: For fixed $\eta_{TR,EX}$, changes in the total efficiency (i.e. additional interception at the *accelerator* level) has a strong influence on the base efficiency. Variations with the modulated Isp, however, appear more lazy, and do not inflict significant losses until some threshold in the vicinity of $c/c_0 = 0.4$.

2. *Variations in* $\eta_{TR,EX}$: For fixed η_{TR}, changes in the extractor transmission seem to have a pronounced effect. This makes sense, given the fact that the extractor is biased, unlike the accelerator, and so additional extractor interception should come with an added penalty (recall the $I\left(1-\eta_{TR,EX}\right)V_{EX}$ term in the power expansion).

3. *Variations in* P: For fixed transmission, changes in the power consumption heavily influence the total efficiency, with the largest powers exhibiting the largest losses. This phenomenon is related to the empirical factor α, the sensitivity of the current throughput to the applied electrostatic field. For fixed α, more power means a stronger field, which tends to necessitate larger V_{EX}, and therefore lead to larger losses because of the penalty for extractor interception. It appears, however, that for larger powers this could be assuaged by larger α, pointing to the possibility of an optimal value that depends upon a given mission or application. Exploration of this idea will be reserved for future work.

All of the information leads to the conclusion that good efficiency performance can only be achieved when high levels of beam transmission prevail in the system. As designers, it should be possible to actively accomplish this through one of two approaches: (1) try to narrow the intrinsic energy distributions of electrosprayed beams, or (2) ensure prudent grid design. While the physics of the former are still an open question, the latter has already proven its effectiveness in the laboratory. Previous investigations with high density electrospray arrays (in particular, the proof-of-concept device to be discussed in the following section) have demonstrated near-unity beam transmission [10], and variable Isp explorations with single emitters have demonstrated a similar quality down to Isp levels of only several hundred seconds [21]. This suggests that future multi-modal devices (e.g. iEPS) should be able to achieve similar levels of performance, and this will facilitate a broad spectrum of feasible Isp (possibly $<$ 1000s to $>>$ 3000s) that can lend significant mission flexibility to CubeSats.

4.3 Proof-of-Concept Demonstration

Several demonstrations of variable Isp electrosprays have previously been described in the literature [21, 23], but these have all been limited to single emitters or small arrays (10s of emitters or less). In practical propulsion scenarios, however, it is likely that many more electrospray sources would need to be arrayed in order to meet the thrust requirements of existing satellites. To demonstrate the constant power, variable Isp concept at this level, a simple experiment was designed to characterize the energy characteristics of the ion plumes being emitted from an iEPS array operating at several different Isp levels.

For the purposes of this demonstration, a porous electrospray array, not unlike the one depicted in Figure 3-3, was manufactured using the techniques outlined in the Fabrication section. This array contained the usual 480 tips, and atop them were suspended two perforated tungsten grids serving as extractor and accelerator. This emitter-grid assembly was mounted within a small vacuum facility and situated in

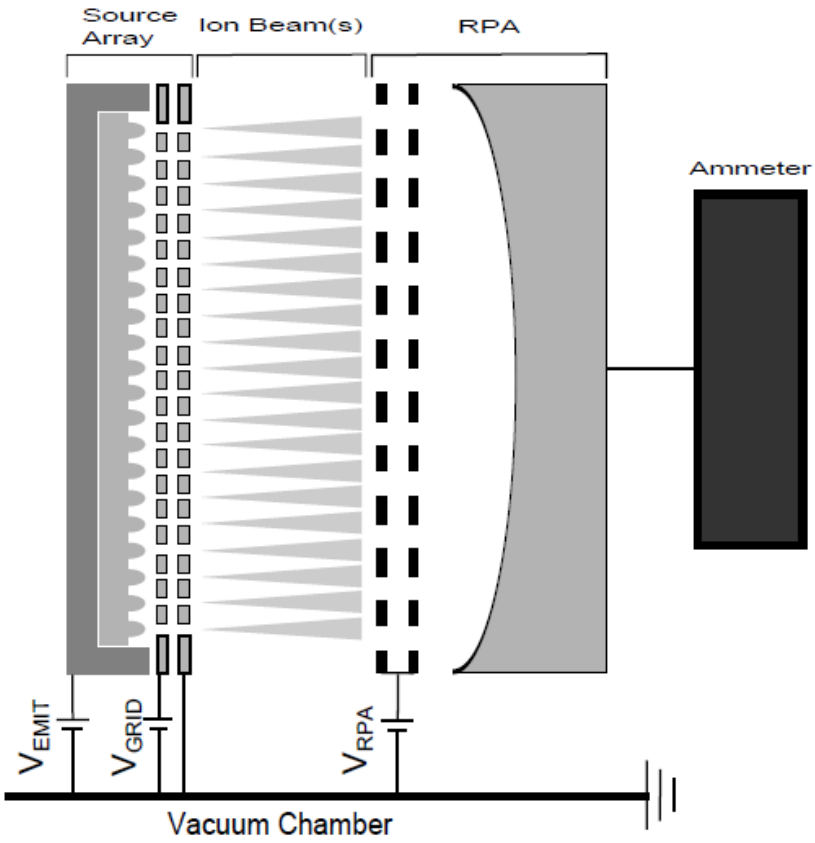

Figure 4-9: Variable Isp test configuration.

front of a Retarding Potential Analyzer (RPA) that was used to monitor the energy profile of the electrosprayed plume. A schematic of this test configuration can be seen in Figure 4-9.

The emitter array, extractor grid, and RPA potentials were each controlled by a Matsusada AMS-5B6 high voltage power supply while the current collected by the RPA was monitored with a Keithley 6517 Electrometer. The emitter and extractor voltages were adjusted manually, in order to investigate several Isp levels while maintaining constant power, whereas the RPA potential was swept from ground to the appropriate emitter potential using an Agilent 33220A function generator during each trial. The energy measurements collected in this process can be seen in Figure 4-10.

Each curve in the figure corresponds to a unique level of Isp, as dictated by the emitter potential, but is linked to each one of the others through the constancy of the

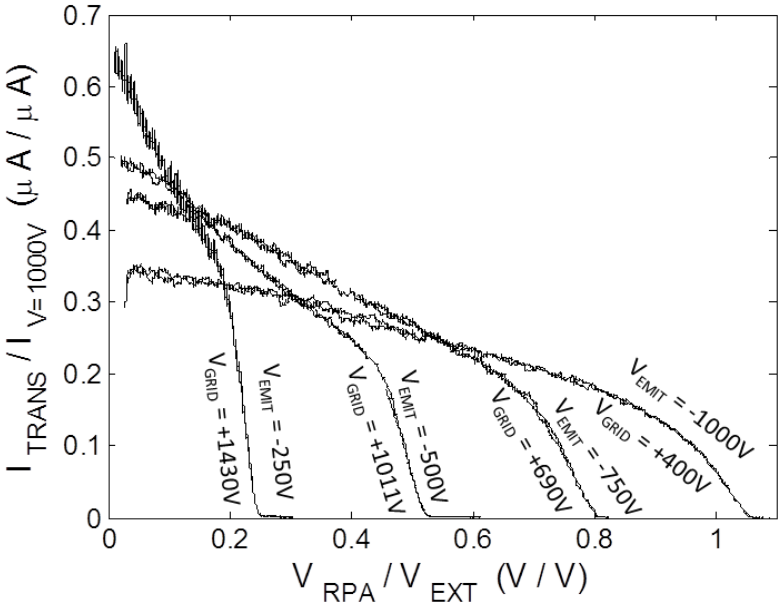

Figure 4-10: Energy measurements for variable Isp experiments. Notice that each curve indicates the presence of a monoenergetic ion population (at the high-energy end), in addition to a population ions with lower and distributed energies within the beam. This phenomenon is related to ion fragmentation.

power that they carry ($\sim$ 13 mW). The ordinate axis depicts the current collected by the RPA while the abscissa represents the associated potential barrier. Though the abscissa values are explicit in the RPA potential, this, again, is related to Isp of the device as described in Eq. (4.8). However, in this case it can be seen that the energies of the individual particles constituting the beam are distributed, rather than monoenergetic. This means that the Isp must be, more generally

$$F = \dot{m}\bar{c} = \int c\, d\dot{m} \Rightarrow \bar{c} = \frac{1}{\dot{m}} \int c\, d\dot{m} \tag{4.27}$$

where $\bar{c}$ is the particle-averaged Isp, $\dot{m}$ is the total mass flow, c is the exhaust velocity specific to each individual particle, and $d\dot{m}$ is the differential mass flow at the local c. Despite this, it is noted that each plume contains some fraction of particles that possess energies very near that which is supplied by the source. This means that the averaged Isp is likely very near, but slightly below, that described by Eq. (4.8). Regardless of their exact values, however, it is clear that the curves, from left to right,

represent a monotonically increasing Isp. Similarly, the lower Isp curves are seen to carry more current than their higher Isp counterparts, and this is indicative of the current/Isp decoupling that was identified for demonstration. As evidence of this decoupling, it suffices to point to the fact that, for single-grid devices, the current and Isp scale together (see Figure 4-3: V_{EMIT} sets both the emission field and the net potential) but the converse is true in this case. Consequently, it is concluded that the current/Isp decoupling necessary for constant power Isp modulation has been successfully demonstrated.

Chapter 5

Conclusions and Future Work

Ultra-small satellites and, in particular, CubeSats have begun to garner significant interest for their economic advantages with respect to larger, more traditional spacecraft. To date, however, the vast majority of CubeSat missions have been restricted to passive activities because they lack means for active propulsion, which is largely unavailable for satellites of their size. This deficit in attractive micropropulsion options can be predominantly attributed to two key issues that have plagued common electric and chemical propulsion systems: (1) the gas-phase ionization and combustion chambers that many EP and chemical engines rely upon possess scaling characteristics that comprise performance at sizes which are amenable to ultra-small satellite integration, and (2) these same engines often require ancillary components, such as electrical pumps and valves, that are difficult to directly miniaturize and/or consume an inordinate amount of the available power budget.

The ion Electrospray Propulsion System (iEPS), is a MEMS-based electrostatic thruster for space propulsion applications. The iEPS concept relies upon a unique ion production mechanism, the electrospray phenomenon, that is fundamentally different from many of its gas-phase EP relatives, and this permits it to operate effectively at scales which are conducive to small satellite purposes. In addition, it takes advantage of a passive propellant feed system and uses a variable Isp mechanism to function in both high thrust and high Isp propulsion capacities. Together, these features have drastically reduced the size of the propulsion footprint in a way that could ultimately

lend feasibility to active CubeSat propulsion.

In this thesis, the iEPS concept has been presented and the physical underpinnings of the mechanisms that allow it to achieve its unique set of characteristics were developed. A proof-of-concept thruster that has previously been used to demonstrate manufacturing feasibility for large, dense arrays of porous electrospray emitters was introduced alongside test results that have shown it to achieve competitive performance without the need for an encumbering footprint. Additionally, the scaling arguments that followed suggest that radically improved thrust production, even eclipsing that of much larger engines, might be possible in the future.

The capability for variable Isp operation was motivated and a mechanism for its realization within electrospray architectures was also introduced and explored. To validate the concept, the results of a simple modulation experiment were shown. In conjunction with theoretical notions for dual-grid engine efficiency, these suggest that future devices should provide broad flexibility to CubeSat missions so long as grid interception can be minimized.

5.1 Future Work

While the theoretical notions and demonstrations presented in this thesis suggest a promising future for multi-modal electrospray engines, a great deal of work remains before iEPS devices reach flight maturity. To facilitate progress toward this goal, the following recommendations for future research should be taken into consideration:

1. *Densification*: Identify the physical limits of densification and begin to pursue them. Direct emitter densification, up to a factor of 2-4, should be readily achievable with existing packaging schemes and might drastically improve overall thrust capabilities.

2. *Electrochemical Fabrication*: Continue building upon the foundation set forth by Courtney [10], and explore the electrochemical fabrication techniques in further detail. The identification of very robust and repeatable manufacturing recipes

will help to expedite the research process by allowing the actual electrospray physics to be considered with greater exclusivity.

3. *Ion Optics*: Investigate the ion optics of ionic liquids and devise models for beam propagation. A thorough understanding of this behavior, which should facilitate the avoidance of some degree of harmful beam interception, is necessary for the prudent grid design that was motivated in Chapter 4.

4. *Grid Fabrication*: The latter item (Ion Optics) can be used to deduce the geometric aspects of efficient grids designs, which will need to be fabricated in a high-fidelity way. The identification of robust and repeatable manufacturing techniques will prove useful in this endeavor.

5. *IL Properties*: Fragmentation was shown to have contributed to the distributed nature of ionic liquid beam energies, which ends up resulting in interception. An understanding as to how and why ILs fragment during the emission process and ionic free-fall will be extremely important in the formulation of strategies for mitigating the detrimental effects of this phenomenon.

Bibliography

[1] C. Venturini, L. Abramowitz, J. Johansen, and J. Gee. Cubesat development programs - working with the community. In *AIAA SPACE 2009*, Pasadena, CA, 14-17 Sept., 2009, AIAA 2009-6501. 13

[2] P. Lozano and M. Martinez-Sanchez. Fundamentals and definitions. In *MIT 16.522 Space Propulsion: Lecture Notes*. 15

[3] J. Mueller, R. Hofer, M. Parker, and J. Ziemer. Survey of propulsion options for cubesats. In *57th JANNAF Propulsion Meeting*, Colorado Springs, CO, 3-7 May 2010, JANNAF-1425. 19

[4] G. I. Taylor. Disintegration of water drops in an electric field. In *Proceedings of the Royal Society of London, Series A: Mathematical and Physical Sciences*, Vol. 280 (1964), No. 1382, pp. 383-397. 22

[5] P. Lozano and M. Martinez-Sanchez. Efficiency estimation of EMI-BF4 ionic liquid electrospray thrusters. In *41st AIAA/ASME/SAE/ASEE Joint Propulsion Conference & Exhibit*, Tucson, AZ, 10-13 July, 2005, AIAA 2005-4388. 25

[6] M. Martinez-Sanchez. Colloidal engines. In *MIT 16.522 Space Propulsion: Lecture Notes*. 28

[7] Paulo C. Lozano. *Studies on the Ion-Droplet Mixed Regime in Colloid Thrusters*. PhD dissertation, MIT, Department of Aeronautics and Astronautics, 2003. 29

[8] G. Lenguito, J. Fernandez de la Mora, and A. Gomez. Multiplexed electrospray for space propulsion applications. In *46th AIAA/ASME/SAE/ASEE Joint Propulsion Conference & Exhibit*, Nashville, TN, 25-28 July 2010, AIAA 2010-6521. 33, 41

[9] B. Gassend, L. F. Velasquez-Garcia, A. I. Akinwande, and M. Martinez-Sanchez. A microfabricated planar electrospray array ionic liquid ion source with integrated extractor. *Journal of Microelectromechanical Systems*, 18(3):679–694, 2009. 33, 41

[10] Daniel G. Courtney. *Ionic Liquid Ion Source Emitter Arrays Fabricated on Bulk Porous Substrates for Spacecraft Propulsion*. PhD dissertation, MIT, Department of Aeronautics and Astronautics, 2011. 33, 36, 37, 41, 42, 59, 63, 68

[11] D. G. Courtney, H. Li, and P. Lozano. Emission measurements from planar arrays of porous ionic liquid ion sources. *Journal of Physics: D, Applied Physics.* 36, 37, 59

[12] S. R. Legge and P. C. Lozano. Electrospray propulsion based on emitters microfabricated in porous metals. *Journal of Propulsion and Power*, 27(2):485–495, 2011. 37, 39, 41

[13] Robert S. Legge Jr. Fabrication and characterization of porous metal emitters for electrospray applications. Master's thesis, MIT, Department of Aeronautics and Astronautics, 2008. 37, 39, 41

[14] M. M. Cepkauskas and J. Yang. Equivalent properties for perforated plates - an analytical approach. In *18th International Conference on Structural Mechanics in Reactor Technology (SMiRT 18)*, Beijing, China, August 7-12, 2005, SMiRT 18-F06-1. 39

[15] J. Harrop and H. M. S. Abdul-Wahab. An experimental study of the rigidity of perforated plates. *Nuclear Engineering and Design 4*, pages 480–489, 1966. 39

[16] D. G. Courtney, H. Li, and P. Lozano. Electrochemical micromachining on porous nickel for arrays of electrospray ion emitters. *Journal of Microelectromechanical Systems.* 41, 42

[17] R. Krpoun and H. R. Shea. Integrated out-of-plane nanoelectrospray thruster arrays for spacecraft propulsion. *Journal of Micromechanics and Microengineering*, (19):1–10, 2009. 41

[18] C. Coffman, D. G. Courtney, F. M. Hicks, S. Jamil, H. Li, and P. C. Lozano. Progress toward a variable specific impulse electrospray propulsion system. In *47th AIAA/ASME/SAE/ASEE Joint Propulsion Conference & Exhibit*, San Diego, CA, 31 July - 03 Aug. 2011, AIAA 2011-5591. 42

[19] Ernst Stuhlinger. *Ion Propulsion for Space Flight.* McGraw-Hill Book Company, New York, 1964. 48

[20] Michael Scott Kimbrel. Optimization of electric propulsion orbit raising. Master's thesis, MIT, Department of Aeronautics and Astronautics, 2002. 48

[21] S. Sumer, P. Lozano, and M. Martinez-Sanchez. Characterization of a variable Isp ionic liquid electrospray thruster beam. In *42nd AIAA/ASME/SAE/ASEE Joint Propulsion Conference & Exhibit*, Sacramento, CA, July 2006, AIAA 2006-4641. 55, 63

[22] Timothy P. Fedkiw. Characterization of an iodine-based ionic liquid ion source and studies on ion fragmentation. Master's thesis, MIT, Department of Aeronautics and Astronautics, 2010. 55

[23] D. G. Courtney and P. C. Lozano. Porous ionic liquid ion source fabrication refinements and variable beam energy experiments. In *45th AIAA/ASME/SAE/ASEE Joint Propulsion Conference & Exhibit*, Denver, CO, August 2009, AIAA 2009-5087. 63